

1 This manuscript is a **preprint** and has been submitted for publication in
2 GEOMORPHOLOGY. Please note that, the manuscript is currently under review and has
3 yet to be formally accepted for publication.

4
5 Subsequent versions of this manuscript may have different content. If accepted, the final
6 version of this manuscript will be available via the 'Peer-reviewed Publication DOI' link on
7 the right-hand side of this webpage.

8
9 Please feel free to contact me with any comments or feedback on our study.

10
11
12
13
14
15
16
17
18
19
20
21
22
23
24
25
26
27
28
29
30
31
32
33
34
35
36

37 **Tectonic controls on geomorphology and spatial distribution**
38 **of monogenetic volcanoes in the Central Southern Volcanic Zone**
39 **of the Andes (Argentina)**

40 Fernanda S. Santos^{a,*}, Carlos A. Sommer^a, Maurício B. Haag^{a,b}, Walter A. Báez^c,
41 Alberto T. Caselli^{d,e}, Alejandro D. Báez^{d,e}

42
43 ^a Instituto de Geociências, Universidade Federal do Rio Grande do Sul, Av. Bento Gonçalves 9500,
44 Porto Alegre, RS, Brazil

45 ^b Department of Earth Sciences, University of Toronto, 22 Ursula Franklin Street, Toronto, ON
46 M5S 3B1, Canada

47 ^c IBIGEO (Universidad Nacional de Salta - CONICET), Av. Bolivia 5150, Salta, Provincia de
48 Salta, Argentina

49 ^d Universidad Nacional de Río Negro, Instituto de Investigación en Paleobiología y Geología, Río
50 Negro, Argentina

51 ^e Consejo Nacional de Investigaciones Científicas y Técnicas (CONICET), Instituto de
52 Investigación en Paleobiología y Geología, Río Negro, Argentina.

53
54 *Corresponding author: F.S. Santos

55 E-mail address: 00316383@ufrgs.br

56
57 **Highlights**

- 58 • Mapping of monogenetic volcanoes in the Southern Volcanic Zones of the Andes
59 • Presence of nine clusters with cinder cones (*strombolian*) and maars
60 (*phreatomagmatic*)
61 • Control of oblique tectonics on vent organization, geomorphology and distribution
62 • Volcano morphology and vent distribution reflect contrasting states of stress
63 • Relative ages suggest waning magmatic activity

64

65

66

67 **Abstract**

68 Monogenetic volcanoes are among the most common volcanic landforms on Earth. The
69 morphology and distribution of small volcanoes can provide important information about
70 eruption dynamics and tectonics. The Southern Volcanic Zone of the Andes (CSVZ)
71 comprises one of the most active magmatic regions on Earth. Characterized by the
72 presence of polygenetic volcanoes and calderas in a complex tectonic setting, this region
73 also hosts hundreds of small, back-arc monogenetic volcanoes. In this contribution, we
74 apply a Geographic Information System (GIS) that combines imagery data and digital
75 elevation models to establish the first comprehensive dataset of monogenetic volcanoes in
76 the CSVZ (38° to 40° S), exploring their eruption dynamics and relationship to tectonic
77 and structural processes. Combining spatial analysis and geomorphological observations,
78 we identify the presence of 356 monogenetic volcanoes distributed into nine clusters, now
79 grouped in the Zapala Volcanic Field (ZVF). The ZVF is marked by the predominance of
80 cinder cones (80%) followed by phreatomagmatic volcanoes (20%), suggesting some
81 influence of external water in the eruption dynamics. Generally, monogenetic vents present
82 a clear association with local and regional lineaments, suggesting a strong structural
83 control on the occurrence of the monogenetic deposits. The higher vent densities are
84 observed in the southern Loncopué Trough, an important extensional feature related to
85 tearing of the subducted Nazca plate underneath the South American Plate. Morphometric
86 parameters of cinder cones indicate variable stress orientations in the CSVZ that possibly
87 results from the oblique tectonics in the region. From north to south, the maximum
88 principal stress rotates from NE-SW to E-W and becomes progressively less constrained as
89 it distances from the current magmatic arc. Based on the relative ages, we map the
90 evolution of monogenetic volcanism through time. Our results suggest a waning in the
91 monogenetic activity in ZVF over time. When compared to monogenetic fields in the
92 Central Andes, the ZVF is marked by higher vent densities and number phreatomagmatic
93 landforms, with the absence of lava domes. This ultimately reflects the contrasting crustal
94 structure and climate conditions of these two regions.

95

96 **Keywords:** Monogenetic volcanism; Geomorphology; Southern Volcanic Zone; Andes;
97 Spatial Analysis; Geographic Information System.

98

99 **1. Introduction**

100 Small monogenetic volcanoes are among the most common volcanic landforms on
101 Earth (Wood, 1979), and they can occur as isolated vents, grouped in volcanic fields, and
102 as parasitic vents associated with polygenetic systems (Fornaciai et al., 2012; Kereszturi
103 and Németh, 2012a; Uslular et al., 2015). These landforms are generally classified
104 according to edifice morphology, which depends on endogenous (e.g., magma composition
105 and volatile content) and exogenous (e.g., structural context, interaction with surface water,
106 terrain slope, and wind intensity) factors (Kereszturi and Németh 2012a; Kervyn et al.,
107 2012, Di Traglia et al., 2014; Németh and Kereszturi, 2015). Because of these controls,
108 several eruption styles are associated with monogenetic volcanoes, including hawaiian,
109 strombolian, and hydrovolcanic (Kereszturi and Németh, 2012b; Németh and Kereszturi,
110 2015; Báez et al., 2017).

111 The morphology of monogenetic volcanoes and their spatial distribution reflect
112 important parameters about the dynamic of the volcanic field and their tectonic controls
113 (e.g., structural control and emplacement dynamics; Bemis and Ferencz, 2017). Several
114 studies have shown that edifice morphology and spatial distribution can be used to identify
115 relevant volcanological and tectonic processes, including eruption dynamics, structural and
116 tectonic settings (Tibaldi, 1995; Kereszturi and Németh 2012a; Haag et al., 2019;
117 Marliyani et al., 2020). In recent years the availability of high-resolution Digital Elevation
118 Models (DEMs) and satellite imagery fostered the remote characterization of monogenetic
119 volcanoes. This approach yielded interesting results, allowing a deeper understanding of
120 volcanology, structural, and tectonic processes related to monogenetic volcanic fields (e.g.,
121 Bruno et al., 2006; Kiyosugi et al., 2012; Németh and Kereszturi, 2015; Haag et al., 2019,
122 Morfulis et al., 2020; Uslular et al., 2021).

123 The central segment of the Southern Volcanic Zone of the Andes (CSVZ)
124 comprises one of the most active magmatic regions on Earth (Stern, 2004). In addition to
125 the presence of polygenetic volcanoes and calderas (e.g., Copahue in Argentina, Callaqui,
126 Antuco and Llaima in Chile), this region also hosts hundreds of small back-arc
127 monogenetic volcanoes (Fig 1). Despite their widespread presence in the area, only a few
128 studies have addressed the occurrence of monogenetic volcanism in the CSVZ (e.g.,
129 Muñoz and Stern, 1989; Lara et al., 2006; Cembrano and Lara, 2009) and none of them
130 deals with the geomorphology of these volcanoes.

131 In this contribution, we use a GIS to report the first complete catalog of
132 monogenetic landforms in CSVZ (henceforth grouped in the Zapala Volcanic Field - ZVF),
133 their morphology, spatial distribution, and structural relationships. Combining satellite
134 imagery and DEMs, we map and classify the monogenetic volcanoes in the region,
135 establishing their eruption dynamics and relationship to tectonic features and processes.

136

137 **2. Geological setting**

138 The CSVZ is located in the southern segment of the Andes and extends between
139 latitudes 37° to 41°5' S, involving regions of Argentina and Chile (Fig. 1). It is part of one
140 of the four volcanic segments associated with the active convergent margin, located on the
141 west coast of South America, where the Cocos, Nazca, and Antarctic plates are subducted
142 by the South American plate (Hickey-Vargas et al., 2002) responsible for the Andean
143 orogeny in the last 200 Ma (e.g., Mpodozis and Ramos, 2008). This zone features hundreds
144 of monogenetic back-arc volcanoes with extensive deposits and variable morphologies, in
145 addition to the presence of numerous large polygenetic systems, such as composite
146 volcanoes and calderas.

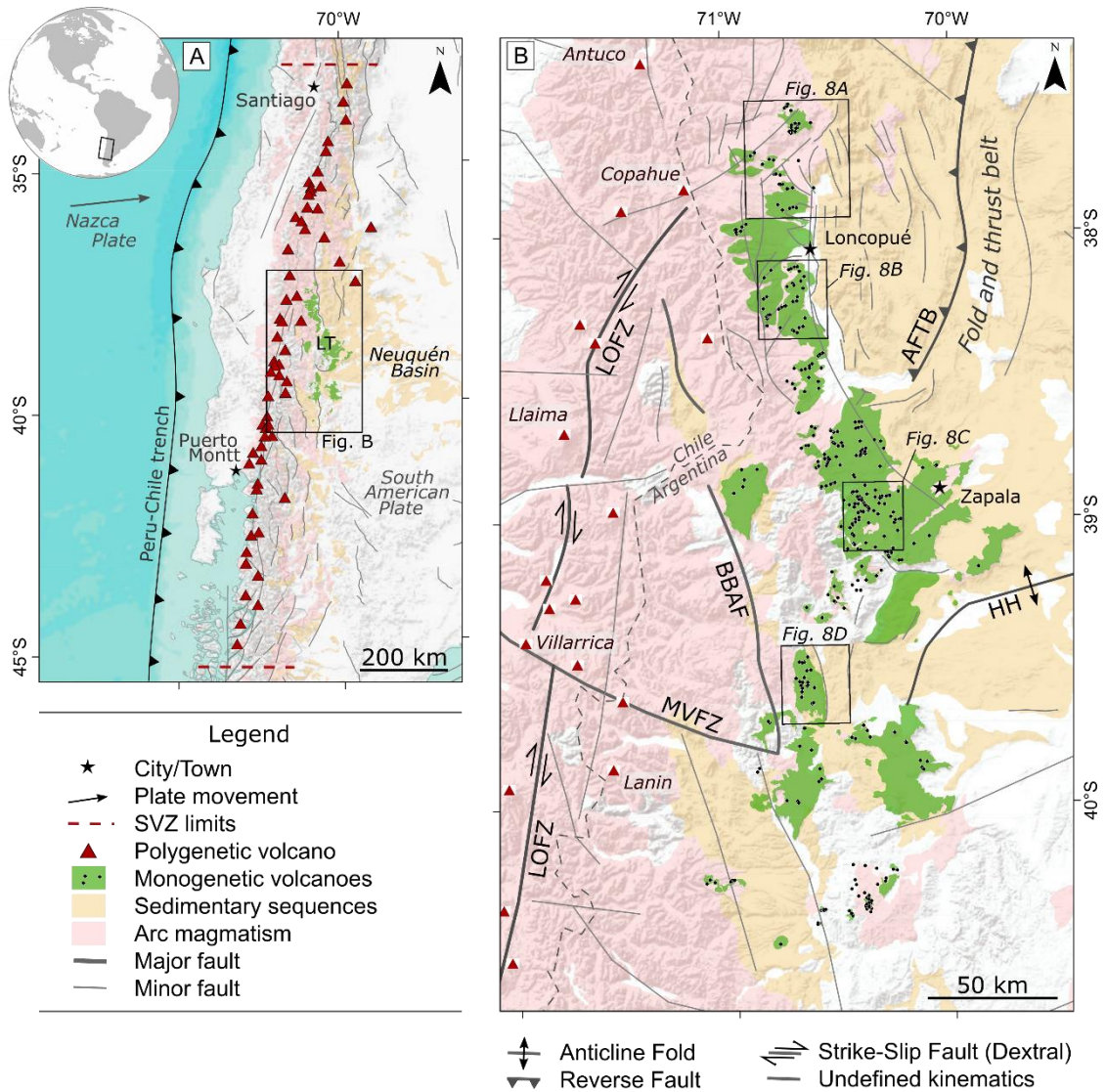
147 The eastern foothills of the Andes between the 31° and 40° S are defined by a
148 significant retroarc basin that comprises a Late Triassic-Early Cenozoic succession called
149 Neuquén Basin (Howell et al., 2005; Fig. 1A). The complex evolution of this basin can be
150 divided in three main phases: (1) the opening of the basin in Late Triassic times, as a result
151 of extensional processes that generated a series of long, narrow depocenters filled with
152 volcanic/volcaniclastic and continental deposits (Vergani et al., 1995; Franzese and
153 Spalleti, 2001; Howell et al., 2005; Carbone et al., 2011), (2) a post-rift phase of thermal
154 subsidence during the Early Jurassic, when an active subduction regime and the magmatic
155 arc are established on the western margin of Gondwana (Franzese et al., 2003; Howell et
156 al., 2005; Mpodozis and Ramos, 2008), and (3) a phase of typical foreland basin between
157 the Late Cretaceous and Early Cenozoic, resulting from the development of a compressive
158 tectonic regime that generated the eastward migration of the orogenic front (Franzese et al.,
159 2003; Howell et al., 2005; Tunik et al., 2010; Gianni et al., 2018).

160 The magmatic activity retreated toward the west in the Oligocene-early Miocene
161 and a series of extensional basins (e.g., Cura Mallín basin) are generated in the foothills of

162 the Neuquén Andes (Radic et al., 2002; Morabito and Folguera, 2005; Ramos and
163 Folguera, 2005). The second period of deformation of the Neuquén Basin and a new
164 expansion of the magmatism to the foreland is produced during the Middle-Late Miocene
165 (Ramos and Folguera, 2005; Kay et al., 2006). The magmatic front begins to retreat again
166 during the early Pliocene, associated with intense volcanic activity and the opening of the
167 Cola de Zorro Basin in the Main Andes between the 37° and 39°S (Vergara and Muñoz,
168 1982; Muñoz and Stern, 1988; Folguera et al., 2006; Ramos and Folguera, 2005).

169 The Pliocene-Quaternary volcanism in the Neuquén region is mainly developed in
170 an N-S belt parallel to the Andean front and the Tromen and Auca Mahuida volcanic fields
171 located further east (Fig. 1B; Folguera et al. 2011). Particularly, a relevant Pliocene-
172 Quaternary activity is focused on the Loncopué Trough (Fig. 1B). This is a narrow, N-S
173 topographic depression of 200 km in length located between the 36°30' and 39°S and
174 limited by the Agrio fold and thrust belt to the east and the volcanic arc to the west
175 (Folguera et al., 2010; Rojas Vera et al., 2010, 2014; Folguera et al., 2011; Pesce et al.,
176 2019). The basal volcano-sedimentary infill of the axial part of the depression starts in the
177 early Pliocene (Cola de Zorro Formation), followed by silicic distal pyroclastic sequences
178 associated with the development of a series of calderas in the west during Pleistocene
179 times, and the posterior emplacement of a basaltic cover in the western sector (Rojas Vera
180 et al., 2014; Pesce, et al., 2019).

181 Finally, significant Pleistocene-Holocene monogenetic basaltic fields develop in the
182 Loncopué Trough, even extending to the Laguna Blanca/Zapala area (~39°S) (Groeber,
183 1928; Varekamp et al., 2010; Folguera et al., 2011; Rojas Vera et al., 2014). These flows
184 consist of olivine-rich basalts that have received different names based on their relative age
185 and location (e.g., Hueyeltué, Huechahue, Malleo, Macho Viejo, Los Mellizos, and Laguna
186 Blanca basalts) (Leanza et al., 1997; Zannettini et al., 2010). Varekamp et al. (2010)
187 analyzed the volcanic centers south of the 37°30'S, including those located around the
188 Laguna Blanca/Zapala area (~39°S), and observed transitional chemical features between
189 intraplate and arc magmas. However, the centers located in the northern sector of the
190 Loncopué Trough showing typical arc signatures (Rojas Vera et al., 2014).



191

192 **Fig. 1.** A) Regional context of the studied area in the Andean Belt; B) regional map of the CSVZ with ZVF
 193 deposits, polygenetic volcanoes, and the main structural features. LT - Loncopué Trough. Structures are:
 194 AFTB - Agrio Fold and Thrust Belt, BBAF - Bío-Bío Fault Zone, HH - Huincul High, LOFZ - Liquiñe-Ofqui
 195 Fault Zone, MVFZ - Mocha-Villarica Fault Zone. Geological units after Cordani et al. (2016).

196

197

198

199

200

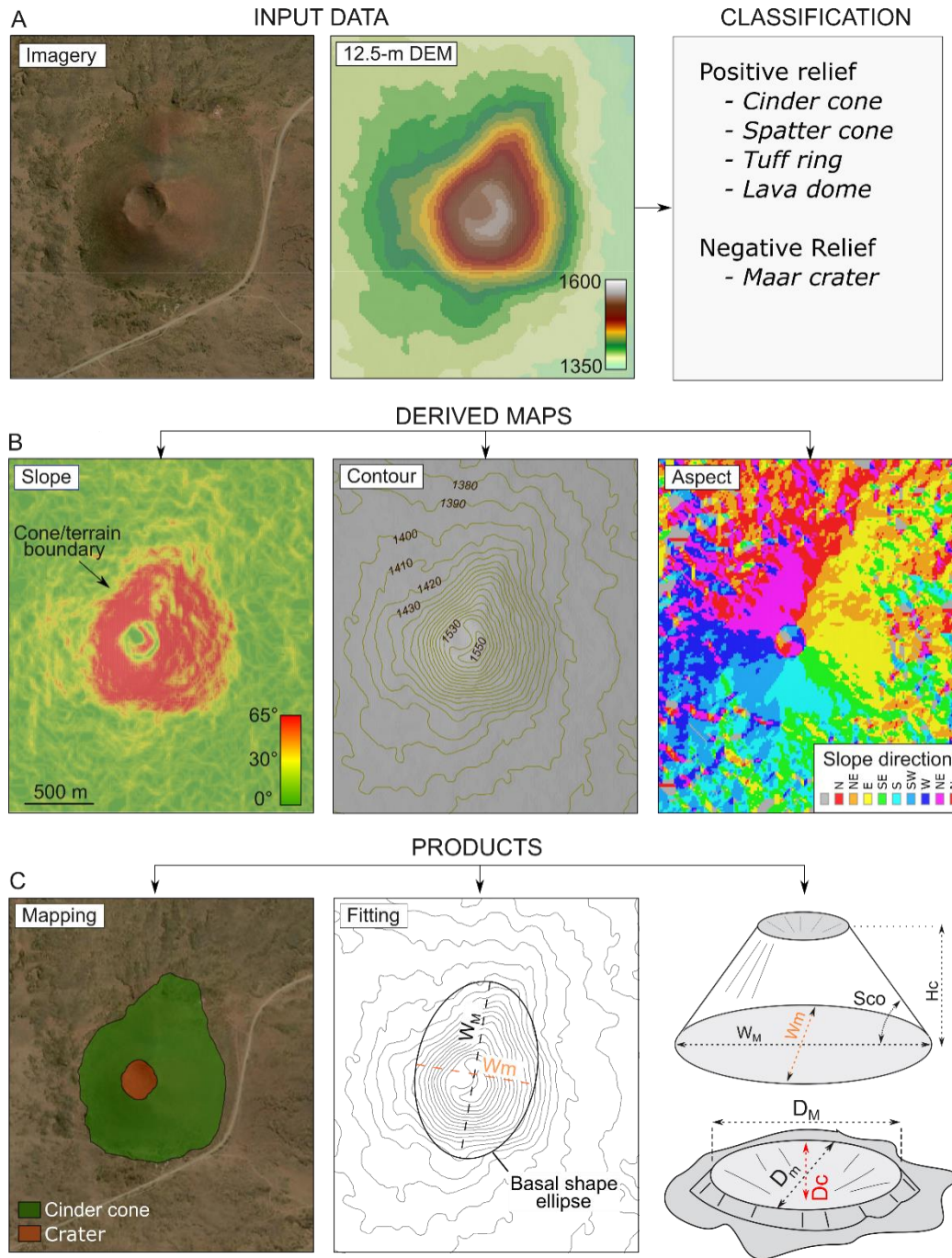
201

202 **3. Methods**203 *3.1. Landform identification, mapping a classification*

204 Monogenetic volcanoes consist of small-volume, nearly circular to elliptical,
205 landforms with either positive (cinder cones, tuff cone, and lava domes) or negative
206 topography (maars - phreatomagmatic structures) (Lesti et al, 2008; Kereszturi and
207 Németh, 2012a; Németh and Kereszturi, 2015; Smith and Németh, 2017; Haag et al.,
208 2019). Based on these criteria, we identified possible monogenetic volcanoes in the study
209 area using Google Earth® (1 to 10 m/px) to establish a primary dataset (Fig. 2A). In this
210 step, we also rely on the available geological maps that contain the distribution of
211 monogenetic deposits (i.e., lava flows) for some regions in the study area (Kay et al., 2006;
212 Melnick and Echtler, 2006; Cembrano and Lara, 2009; Varekamp et al., 2010; Rojas Vera
213 et al., 2014; Pesce et al., 2019, 2020).

214 This preliminary dataset was then verified using satellite imagery in ArcMap®. In
215 this process, the landforms were classified in the following categories: cinder cone, maar,
216 tuff ring, tuff cone, and lava dome (Fig. 2A), following the categories proposed by
217 Kereszturi and Németh (2012a) and Németh and Kereszturi (2015). Using this approach,
218 we find out that monogenetic volcanoes in the study area are either cinder cones or maars.
219 To characterize these volcanoes and perform the geomorphological measurements, we used
220 a high-resolution (12.5 m/px) DEM derived from the ALOS PALSAR sensor, which
221 provides full coverage of the studied area and can be freely downloaded at the Alaska
222 Satellite Facility website (available at <https://vertex.daac.asf.alaska.edu/>). To ensure
223 consistency the DEM was set to an equal-area projection (UTM 19S).

224 From the DEM we used ArcMap® 10.5 to derive several terrain attributes,
225 including slope, contour, and aspect (Fig. 2B), which are useful for mapping the
226 monogenetic volcanoes. Based on these maps and satellite images, we performed a
227 supervised (i.e., manual) geomorphological mapping of the volcanoes and their associated
228 deposits (at a local scale of 1:10,000, Fig. 2C to the left). Based on the mapping and the
229 contour plots, we performed an ellipse fitting and the morphometric measurements using
230 ArcMap Spatial Analyst (Fig. 2C, to the center).



231

232 **Fig. 2.** Methodology applied to this study: A) imagery and DEM (elevation scale in meters) comprise input
 233 data, which were used to identify and classify the monogenetic landforms; B) DEM-derived maps include
 234 slope (scale in degrees), contour (10-m interval curves) and aspects (slope direction); C) supervised (manual)
 235 mapping, ellipse fitting and measurements of the monogenetic landforms. Abbreviations are W_M - Cone
 236 maximum basal width; W_m - Cone minimum basal width; H_c - cone height; S_{co} - cone flank slope; D_c - maar
 237 crater depth; D_M - maximum diameter of maar crater; D_m - minimum diameter of maar crater.

238

239 For cinder cones, we measured the maximum basal width (W_M), minimum basal
240 width (W_m), height of the cone (H_c), and maximum flank slope (S_{co}) (Fig. 2C). For maar
241 volcanoes, we measured the depth of the crater (D_c), as well as the maximum (D_M) and
242 minimum crater diameter (D_m) (Fig. 2C). We also take the azimuth of the maximum
243 diameter W_M and D_M , which is better explained in section 3.3. *Morpho-structural analysis*.

244 3.2. *Spatial analysis*

245 The spatial analysis allows the identification of the degree of clustering, the
246 detection of subclusters, and the internal organization of the monogenetic vents. After
247 mapping and classification of the targets, point analyzes were performed using the spatial
248 analysis tools in ArcMap® applying the methodology proposed by Bishop (2007).

249 The identification of the number of monogenetic clusters in ZVF was based on the
250 methods of Cañón-Tapia (2016), using kernel density functions. According to the search
251 radius, the number of detected clusters follows a power-law distribution in which the
252 inflection point indicates the optimum number of clusters within a monogenetic field
253 (Cañón-Tapia, 2016; Morfulis et al., 2020).

254 The distribution pattern within each monogenetic cluster was analyzed using the
255 Average Nearest Neighbor (ANN) analysis (Bruno et al., 2004). In this method, the
256 *observed* distance among monogenetic vents (R_o) in a given area (A_{HULL}) is compared to
257 the *expected* distance of evenly distributed vents (R_e). The R-statistic parameter results
258 from the R_o/R_e ratio and indicates whether the points distribution follows a Poisson (R-
259 statistic = 1), clustered (R-statistic \rightarrow 0.0), or dispersed (R-statistic \rightarrow 2.0) distribution
260 (Bishop, 2007).

261 3.3. *Morpho-structural analysis*

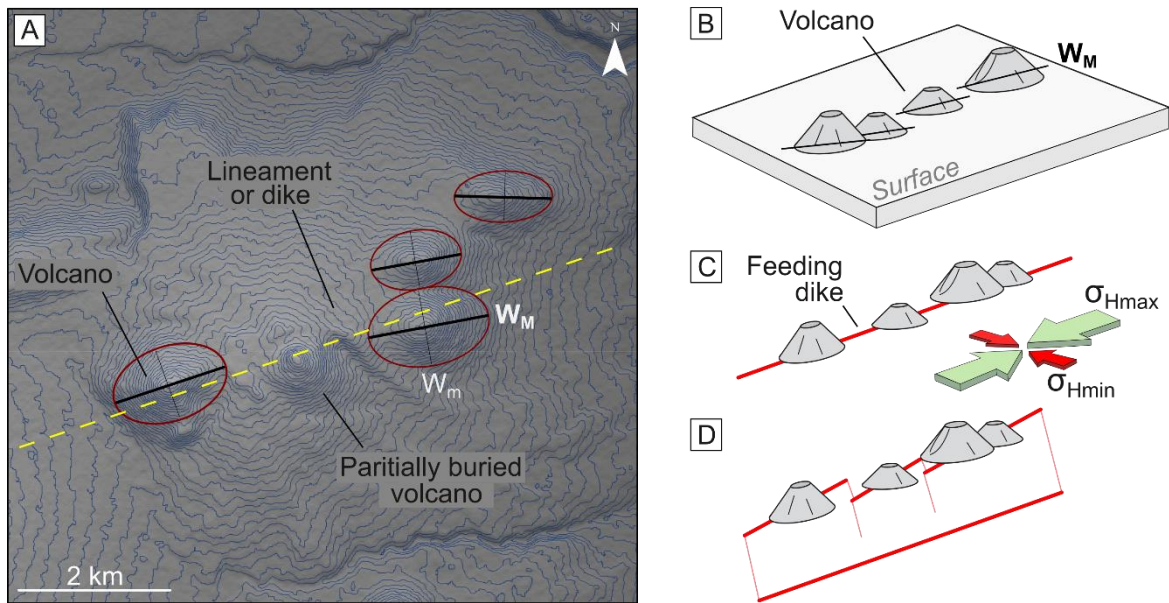
262 The determination of stress state can be inferred from the spatial distribution of
263 monogenetic vents and their main attributes (Fig. 3; Tibaldi, 1995; Paulsen and Wilson,
264 2010; Bonali et al., 2011; Le Corvec et al., 2013; Tadini et al., 2014; Haag et al., 2019;
265 Marliyani et al., 2020; Morfulis et al., 2020). In this context, the surface distribution of
266 monogenetic volcanoes and their elongation (Fig. 3A, B; Tibaldi, 1995) can be used to
267 infer the orientation of subsurface structures, such as dike, fractures, and faults, which
268 ultimately reflect the local stress state (Fig. 3C, D).

269 To determine the relationship between monogenetic vents and the structural setting
270 in the ZVF we followed a similar approach to Tibaldi (1995) and Bonali et al. (2011),
271 using morphometrics to infer the states of stress.

272 To this end, we measure directional parameters for each monogenetic volcano
273 using ellipses (Fig. 3A) and measuring the basal elongation of cones (azimuth of W_M) and
274 crater elongation of maars (azimuth of D_M). We also calculate the ellipticity for both cones
275 and maars by dividing the minimum for the maximum diameter of these features ($W_m/$
276 W_M ; Tibaldi, 1995). In the case of cinder cones, we did not measure crater elongation and
277 crater-rim depressed points (e.g., Tibaldi, 1995) because these features are either absent or
278 not completely clear in most of the studied cones in the ZVF.

279 Finally, we also measured alignments of both cinder cones and maars. Vent
280 alignment/dike presence was determined using at least three vents, and by observing the
281 presence of elongated cones ($W_m/ W_M < 0.8$) or dikes (Fig. 3A), following the
282 recommendations of Le Corvec et al. (2013) and Paulsen and Wilson (2010). In this study,
283 we did not use densities plots to infer conduit and dike orientations (e.g., Cebriá et al.,
284 2011; Tadini et al., 2014) because it generally neglects morphometric and field evidence
285 that result in more robust results (Paulsen and Wilson, 2010).

286 Both vent alignment and the basal elongation of monogenetic volcanoes/maar
287 craters are parallel to the maximum horizontal stress (σ_{Hmax}) and perpendicular to the
288 minimum horizontal stress (σ_{Hmin}), as suggested by several studies (Fig. 3C; e.g.,
289 Nakamura et al., 1977; Tibaldi, 1995; Lara et al., 2006; Haag et al., 2019; Marliyani et al.,
290 2020). Monogenetic cones may also be slight oblique to the main feeding system,
291 suggesting an *en echelon* distribution (Fig. 3D). In the structural analysis we only consider
292 cones emplaced in flat surfaces (slope $< 5^\circ$) and without significant modification (i.e.,
293 extensively degraded cones and maar craters).



294

295 **Fig. 3.** Morpho-structural and lineament analysis. A) Hillshade image with contours used for ellipse fitting
 296 and measurement of W_M and W_m for cones or D_M and D_m for maars - cone height; B) sketch of the surface
 297 expression of monogenetic cones; C) subsurface sketch of inferred plumbing system based on cone basal
 298 elongation for normal faulting; D) subsurface sketch of inferred plumbing system for strike-slip and *en*
 299 *echelon* geometries; σ_{Hmax} - maximum horizontal stress; σ_{Hmin} - minimum horizontal stress.

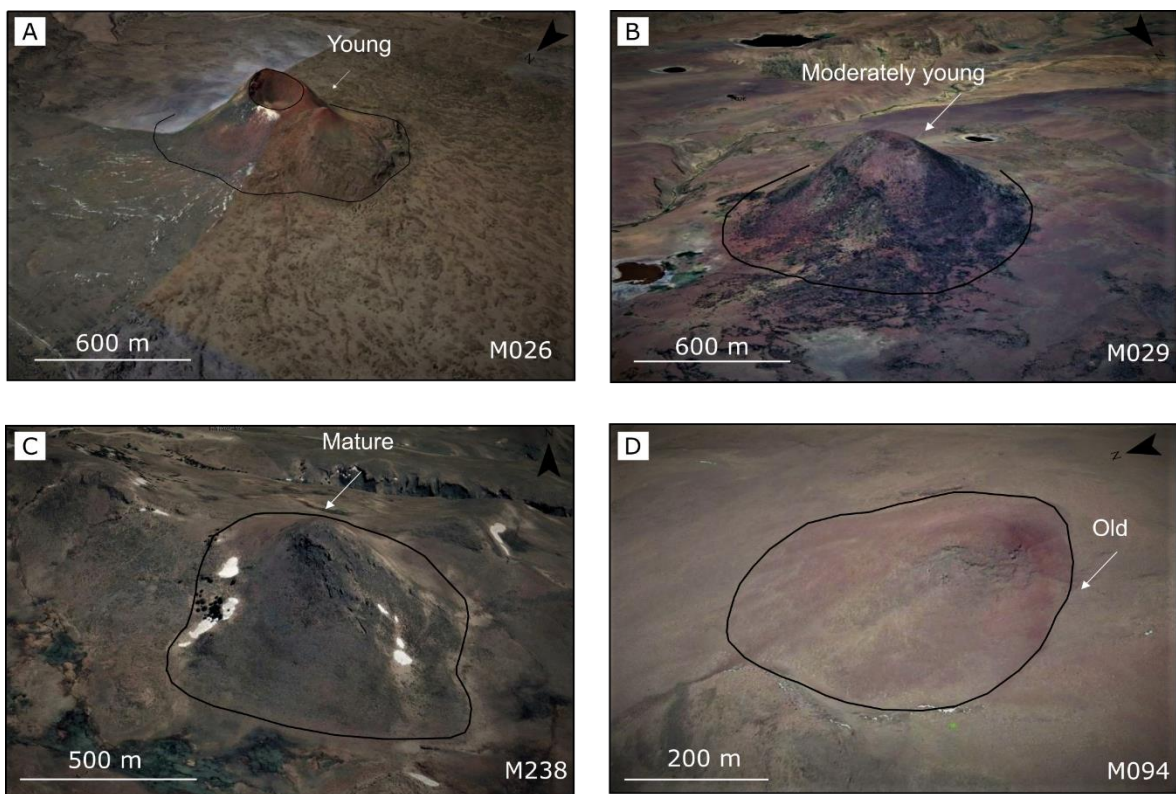
300

301 3.4. Relative age

302 In monogenetic fields, the number and distribution of active volcanoes can vary
 303 over time (Le Corvec et al., 2013). Differently from other regions in the Andes that have
 304 extensive well-dated ignimbrite deposits and abundant radiometric ages, thus allowing a
 305 better constraint on the spatial evolution of the magmatism (e.g., the Central Andes,
 306 Tibaldi et al., 2017), the volcanoes in the ZVF do not have this database yet.

307 As an alternative to determine the spatio-temporal evolution of monogenetic
 308 volcanism in the ZVF, we assigned relative ages to the cinder cones based on
 309 morphometric attributes including crater, cone, and lava flow integrity. These attributes
 310 reflect modification stages to the original, conical shape of cinder cones and are mainly
 311 based on simulation and geomorphological observations (Hooper and Sheridan, 1998;
 312 Fornaciai et al., 2012; Kereszturi and Németh, 2012b; Zarazúa-Carbajal and Cruz-Reyna,
 313 2020).

314 Following this approach, cinder cones were grouped into four categories (Fig. 4),
 315 following an adaptation of the methods of Haag et al. (2019): young - cinder cones with
 316 well-defined craters and basal limits, smooth surfaces, and absence of erosional features;
 317 moderately young - cones without a well-defined crater and roughly defined basal limits,
 318 with deep and well-established gullies and rills; mature - cones without a well-defined
 319 crater and roughly defined basal limits, with ravines and rills; old - reduced landforms,
 320 without a defined crater basal limit, cut by deep ravines and rills. Using this classification
 321 method, we created regional maps of relative age in the studied area, comparing our results
 322 with the available absolute ages from the literature (e.g., Ramos and Folguera, 2005).



323
 324 **Fig. 4.** Relative age classes of studied cinder cones. A) young (coordinates are 39° 01' 22.76" S; 70° 22'
 325 28.88" O); B) moderately young (38° 58' 37.84" S; 70° 24' 31.40" O); C) mature (38° 53' 30.92" S; 70° 33'
 326 43.71" O); D) old (37° 59' 20.14" S; 70° 56' 31.35" O). Relative scale due to perspective. Vertical
 327 exaggeration of 3. Source: GoogleEarth (2021).

328

329

330

331

332 4. Results

333 4.1. Geomorphology and morphometry

334 We identify 336 monogenetic volcanoes in the study area, with a predominance of
335 cinder cones (80%) followed by phreatomagmatic (maars) volcanoes (20%). Monogenetic
336 deposits (volcanoes and their associated lava flows) cover approximately 6.400 km² in the
337 CSVZ. The main morphological attributes are represented in Fig. 5, while the distribution
338 of monogenetic volcanoes and their main morphometric parameters are reported in Fig.
339 6A. All elevations are reported in meters above sea level (a.s.l).

340 4.1.1 Cinder Cones

341 Cinder cones are the predominant landforms in the ZVF and exhibit a significant
342 variation in their geomorphologic attributes (Fig. 5A, B, C). They are frequently breached,
343 elongated edifices associated with extensive lava flows (Fig. 5A). In several cases, multiple
344 generations of lava flows are observed, suggesting multiple eruptions in the same region
345 (Fig. 5A). A few cinder cones occur nested inside maar craters that cut older lava flows
346 (Fig. 5B). Several cones form clusters that can be grouped by lineaments and are possible
347 related to dikes and feeding systems (Fig 5C).

348 Cinder cones occur throughout the entire study area (Fig. 6A, B), at terrain
349 elevations ranging from 900 to 2,200 m a.s.l. (Fig. 6B). They dominate the northern section
350 (above ~ lat. 39°S) and higher terrain elevations (> 1,600 m a.s.l.) (Fig. 6A, B, C). Below ~
351 lat. 39°S, the presence of maar volcanoes becomes more relevant (Fig. 6A, B, C).

352 The cinder cones also exhibit a significant variation in their morphometric
353 parameters (Fig 6E). Maximum basal widths (W_M) range from 246 to 3,590 m and cone
354 heights (H_c) from 7 to 426 m (Fig. 6E). Most cinder cones are generally elliptical, with
355 W_M/W_M ratios ranging from 1.0 (circular) to 0.4 (highly elliptical) and clustering around
356 0.80 (Fig. 6E). Flank slope angles (S_{co}) from 6 to 40°. For a full report on the
357 morphometric attributes please check Supplementary item 1.

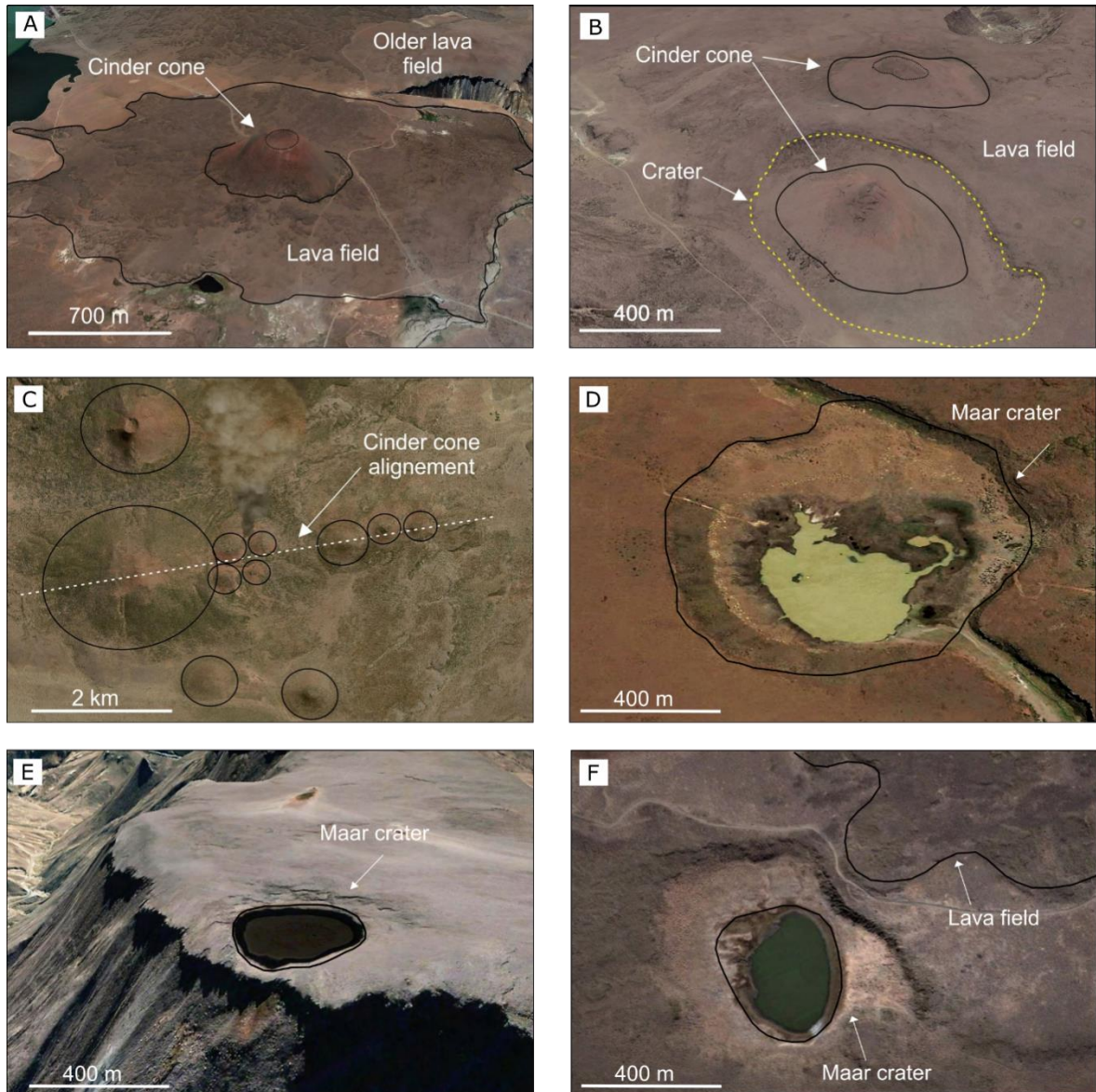
358 4.1.2 Phreatomagmatic volcanoes: maar

359 Maar volcanoes are marked by well-preserved, generally circular craters, partially
360 filled by alluvial sediments and saltpans (Fig. 5D, E, F). Crater limits are roughly delimited

361 by small changes in elevations, because ZVF maars often lack external tephra rings and
362 deposits (Fig. 5D, E, F). Maar craters commonly cut lava plateaus (Fig. 5E) and are closely
363 associated with cinder cones (Fig. 5F).

364 Maar volcanoes are preferentially present south of lat. 39° S (Fig. 6A, B) and at
365 terrain elevations below 1,600 m a.s.l (Fig. 6C). A summary of their main morphometric
366 parameter is presented in Fig. 6F. The depth of the crater (D_c) ranges from 1 to 211 m, and
367 crater maximum axis (D_M) ranges from 142 m to 4,900 m (Fig. 6F). Maar craters are often
368 elliptical to nearly circular, with D_m/D_M ratios ranging from 0.99 (circular) to 0.39 (highly
369 elliptical), while most D_m/D_M ratios are below 0.75 (Fig. 6F). For a full report on the
370 morphometric attributes please refer to the Supplementary item 1.

371

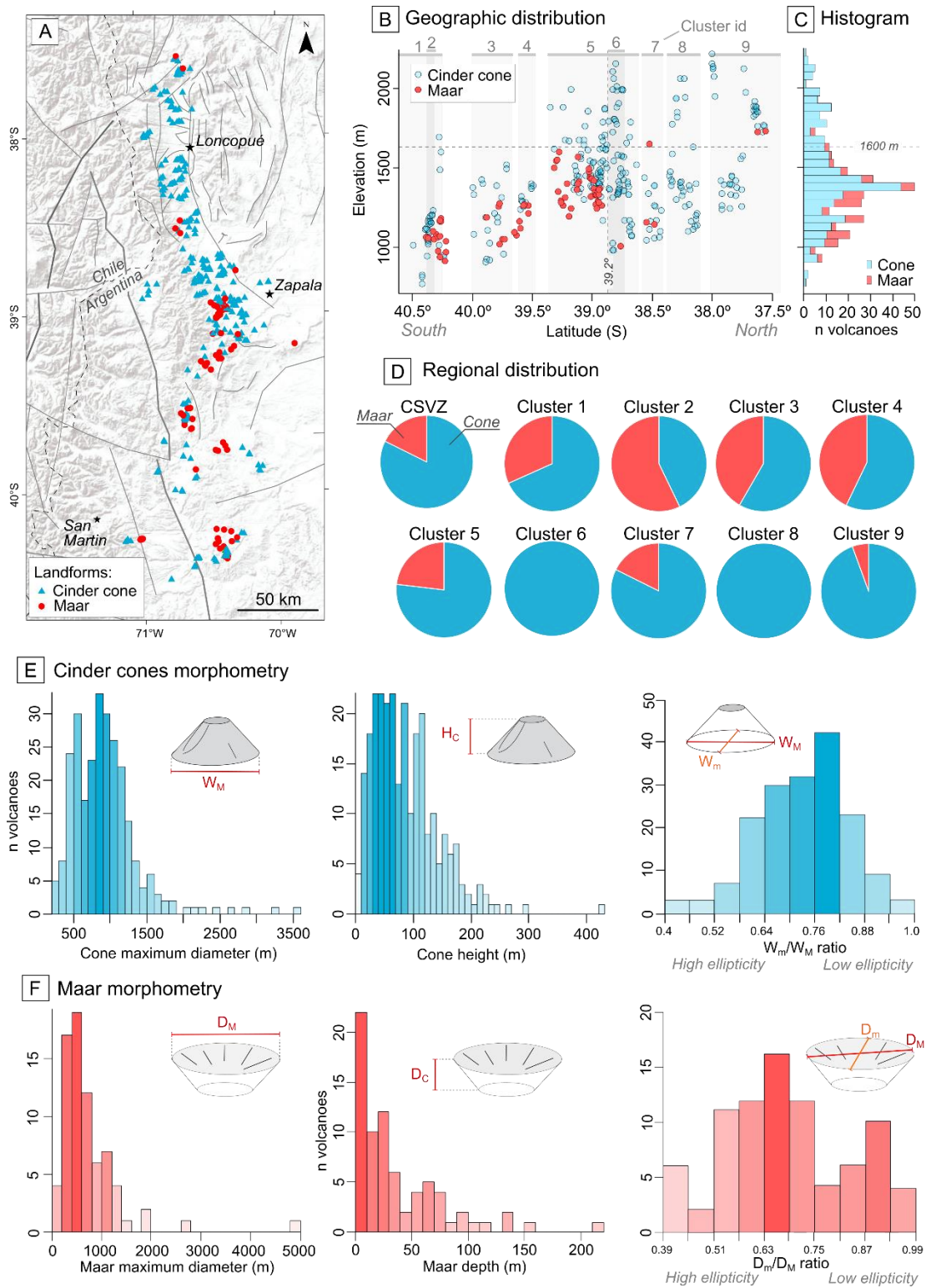


372

373 **Fig. 5.** Representative monogenetic landforms in the CSVZ: A) Cinder cone with associated lava flow (39°
 374 $05' 32.90''$ S; $70^{\circ} 23' 16.80''$ O); B) cinder cone emplaced inside a maar-crater ($39^{\circ} 09' 18.90''$ S; $30^{\circ} 14'$
 375 $25.11''$ O); C) composite alignment of multiple cinder cones ($38^{\circ} 55' 59.42''$ S; $70^{\circ} 20' 28.09''$ O); D) maar
 376 crater emplace on top of thin volcanic sequences ($39^{\circ} 46' 19.97''$ S; $70^{\circ} 22' 54.39''$ O); E) Maar crater
 377 emplace over volcano-sedimentary ($39^{\circ} 16' 19.83''$ S; $70^{\circ} 33' 42.16''$ O); F) Maar craters associated with
 378 cinder cones ($39^{\circ} 35' 47.31''$ S; $70^{\circ} 37' 54.10''$ O). Relative scale due to perspective. Vertical exaggeration of
 379 3. Source: GoogleEarth (2021).

380

381



382

383 **Fig.6.** Morphometric results. A) CSVZ map with the distribution of monogenetic landforms in the ZVF; B)
 384 North to the south geographic distribution of cinder cones and maars; C) histogram with the terrain elevation
 385 of cinder cones and maars; D) landform distribution of wet (represented by maars) and dry (represented by
 386 cinder cones) monogenetic landforms across the ZVF; E) Morphometric results (W_M , H_C , and ellipticity) for
 387 cinder cones; F) Morphometric results (D_C , D_M , and ellipticity) for maar volcanoes.

388 *4.2. Spatial distribution*

389 Spatial analysis was performed using Kernel density estimations for cluster
390 identification and Average Nearest Neighbor (ANN) analysis for pattern determination.

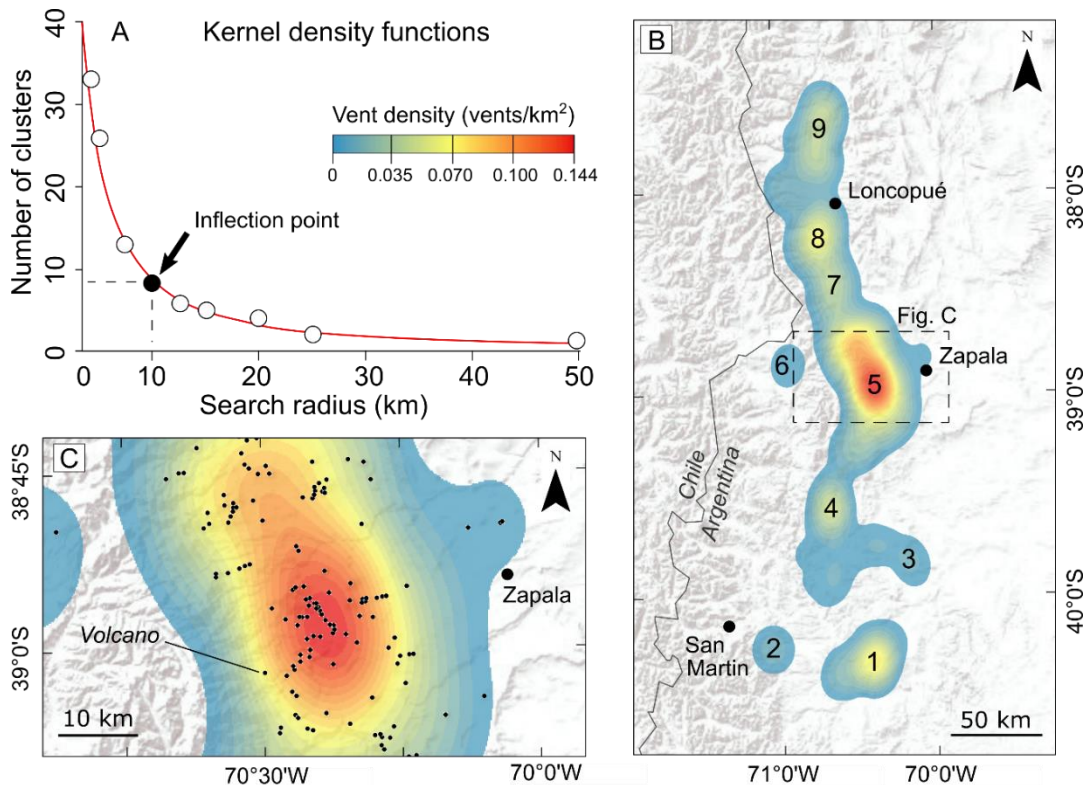
391 *4.2.1. Cluster identification*

392 The identification of the number of the monogenetic clusters was based on the
393 methods of Cañón-Tapia (2016). Following this method, we observe an inflection point at
394 ~10 km (Fig. 7A; Cañón-Tapia, 2016; Morfulis et al., 2020). This value suggests a total of
395 9 monogenetic clusters (Fig. 7A, B) in the CSVZ. The vent density of each cluster is
396 presented in Table 1. The maximum density of monogenetic volcanoes (0.144 vents/km²)
397 is located in cluster number 5 (Fig. 7B), about 30 km southwest of Zapala town (Fig. 7C),
398 at the southern segment of the Loncopué Trough.

399 *4.2.2. Distribution pattern*

400 ANN analysis indicates a strong clustered pattern for ZVF, with an overall R-
401 statistic of 0.392. A summary of ANN results is presented in Table 1. Individually, each
402 monogenetic group presents variable distribution patterns, from clustered to dispersed (Fig.
403 8A, B). A clustered pattern is observable in groups 1, 5, and 9 (Fig. 8A), which present R-
404 statistic ranging from 0.719 (less clustered) to 0.648 (most clustered), all well above the -
405 2 σ range (Fig. 8A, B). The dispersed pattern is recorded in groups 2, 4, 6, and 7, with R-
406 statistic from 1.22 (less disperse) to 2.30 (most dispersed). Groups 4 and 7 are above 1.65 σ ,
407 while groups 2 and 6 above 2.85 σ (Fig. 8A, B). The Poisson pattern is detected only in
408 groups 3 and 8 (Fig. 8A).

409



410

411 **Fig. 7.** Kernel density analysis. A) Number of kernel clusters as a function of the search radius; B) regional
 412 map with identified monogenetic clusters; C) detail map of cluster 5 showing the internal distribution of
 413 monogenetic vents in the southern Loncopué Trough.

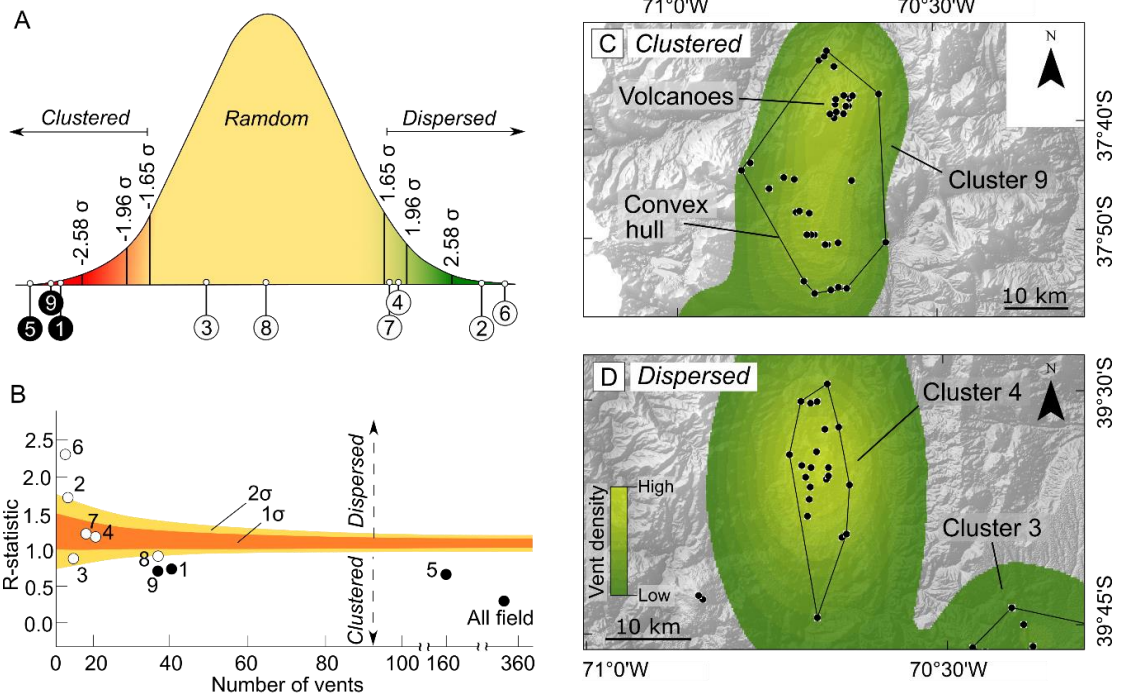
414

415 The spatial pattern and distribution of monogenetic volcanoes is better observed in
 416 detailed maps of each monogenetic group. Group 9 displays strongly clustered
 417 monogenetic vents (Fig. 8A). These vents form in sub-clusters inside the group perimeter
 418 (defined by the convex hull), in E-W trends to the southwest (inferred to be controlled by
 419 local structures), and isotropic groups to the north (Fig. 8C). In contrast, group 4 presents
 420 an opposite spatial pattern, with vents randomly dispersed inside the group area (Fig. 8D).

421

422

423 **Fig. 8. (below)** Summary of ANN analysis. A) normal distribution with confidence intervals and the R-
 424 statistic for each monogenetic cluster; B) plot of R-statistic and number of vents; C) clustered pattern (R-
 425 statistic ~ 0.687), cluster number 9, and the respective convex hull area; D) dispersed pattern (R-statistic \sim
 426 1.21), cluster number 4, and the respective convex hull area.



427

428

429 **Table 1.** Spatial analysis results. ANN patterns are clustered (C), Poisson (P), and dispersed (D).

Parameters	Entire ZVF	Cluster number								
		1	2	3	4	5	6	7	8	9
Vents	355	41	7	12	21	160	5	17	37	37
Area (km ²)	22.510	517	10	194	119	3.009	33	126	358	649
Average density (vent/km ²)	0.015	0.07	0.70	0.06	0.17	0.053	0.151	0.134	0.103	0.057
Maximum density (vent/km ²)	0.144	0.059	0.014	0.013	0.043	0.144	0.010	0.037	0.056	0.037
Re (m)	4,932	2,347	758	2,343	1,436	2,564	1,737	1,700	1,672	2,519
Ro (m)	1,938	1,688	1,276	2,061	1,746	1,663	4,010	2,048	1,668	1,731
R-sta	0.392	0.719	1.683	0.879	1.21	0.648	2.307	1.222	0.997	0.687
Pattern	C	C	D	P	D	C	D	D	P	C

430

431

432

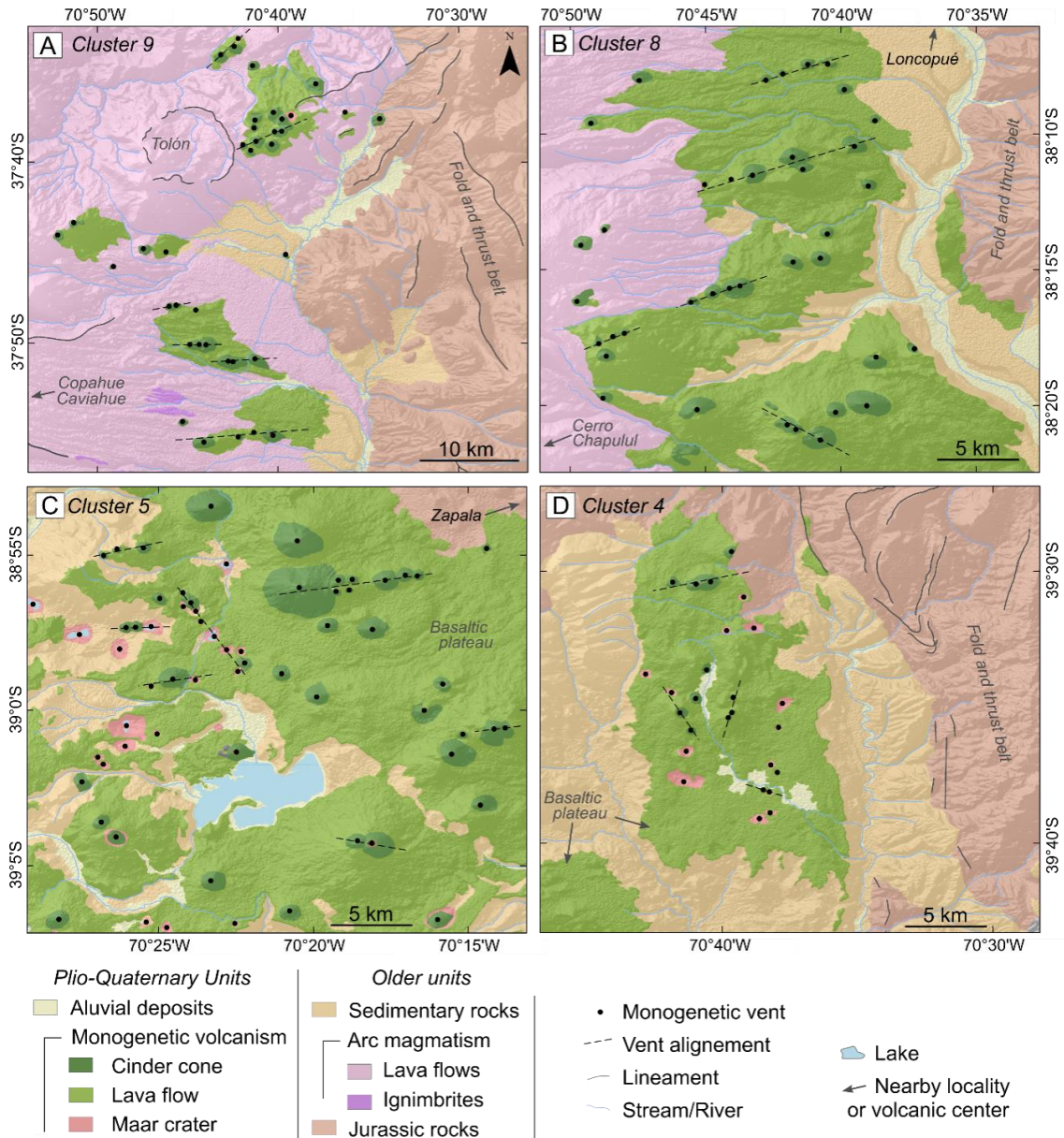
433

434 *4.3. Structures and lineaments*

435 Based on the satellite imagery and the available geological maps (e.g., Rojas Vera
436 et al., 2014; Pesce et al., 2019), we map the occurrence of monogenetic centers in the study
437 area and their relationship with structural features. A summary of the main structural
438 settings observed in the ZVF is provided in Fig. 9. Structural data obtained from cone
439 elongation and vent alignment indicate the predominance of E-W, ENE-WSW to WNW-
440 ESE structures in the ZVF, with significant variations among the different clusters (Fig. 9).

441 Cluster 9 is the closest to the volcanic arc (~ 30 km considering the main trend of
442 active polygenetic volcanoes) and is marked by monogenetic volcanoes mainly associated
443 with E-W structures (Fig. 9A). The northern limit of cluster 9 is characterized by NE-SW
444 alignments, next to the Trolón Caldera (Fig. 9A). Cluster 8 presents a slight change in vent
445 alignment direction when compared to cluster 9, with most features trending ENE-WSW to
446 WSW-ENE (Fig. 9B). Further south, cluster 5 is also marked by ENE-WSW to WSW-
447 ENE trending vents (Fig. 9C). Several NW-SE trending monogenetic volcanoes are also
448 present in the region (Fig. 9C). South of this region, the orientation of vents starts to
449 become more scattered. Cluster 4 shows a variety of orientations, including ENE-WSW,
450 WNW-ESE, NE-SW, and NE-SE trending volcanoes and alignments (Fig. 9D).

451 A summary of the quantitative structural data extracted from monogenetic
452 volcanoes (cone and maar elongation, vent alignment, and dike orientation) is presented in
453 Fig. 10. From north to south, there is an increase in the scattering of the basal cone
454 orientation, as well as vent alignment (Fig. 10A). Despite this, histograms indicate a
455 predominance of ENE-WSW elongated cones in the ZVF following azimuths ranging from
456 80 to 95° (Fig. 10B). This orientation is also confirmed by histograms of vent alignment
457 and the orientation of dikes (Fig. 10C). If we consider the basal ellipticity values (W_m/W_M
458 ratios) and exclude the nearly circular features (W_m/W_M ratios > 0.8), it is interesting to
459 note that we still obtain similar results, with higher kurtosis (i.e., more values close to the
460 mean, Fig. 10D). Maar data indicate the presence of highly elliptical craters (low D_m/D_M
461 ratios) mainly oriented along with ENE-WSW and WNW-ESE directions (Fig. 10E, F).



462

463 **Fig. 9.** Maps of monogenetic volcanoes in the ZVF and their structures, from north to south. A) cluster 9,
 464 with mainly E-W and subordinate NE-SW trending vents; B) cluster 8 with a predominance of NE-SW
 465 trending vents; C) southern section of Cluster 5, with E-W and NW-SE trending volcanoes; D) Cluster 4,
 466 with WSW-ESE, ENE-WSW, NNE-SSW, and NNW-SSE trending vents. Geological units based on Rojas
 467 Vera et al. (2014) and Pesce et al. (2019).

468

469 Rose diagrams built from these data allow better visualization of the orientation of
 470 monogenetic features in the ZVF (Fig. 10G). ENE-WSW to E-S directions prevail among
 471 the main orientations for basal cone elongation, vent alignment, and dike orientation (Fig.
 472 10G). In contrast, the orientation of maar craters shows a higher dispersion when compared

473 to cinder cones, with crater elongation ranging from ENE-WSW to WNW-ESE (Fig. 10G).
474 These results contrast with the main lineaments observed in the fold and thrust belt region,
475 which is marked by the predominance of N-S structures (Fig. 10G)

476 Deviations in basal cone orientation are also observed within each cluster (Fig.
477 10H). Clusters 1, 4, and 6 tend to show a more scatter pattern, while clusters 3, 5, 7, and 8
478 are marked by a predominance of E-W trending cones (Fig. 10H). Cluster 9 is the closest
479 to the current volcanic arc (Fig. 9A) and presents a bimodal distribution of cinder cones
480 basal elongation (Fig. 10H).

481

482

483

484

485

486

487

488

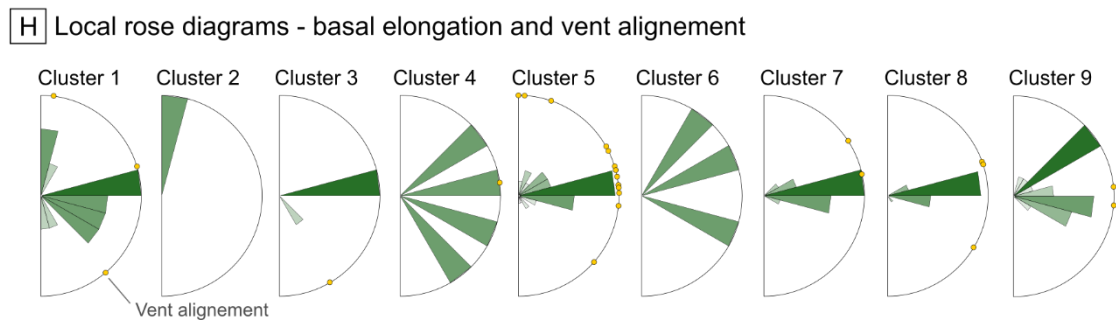
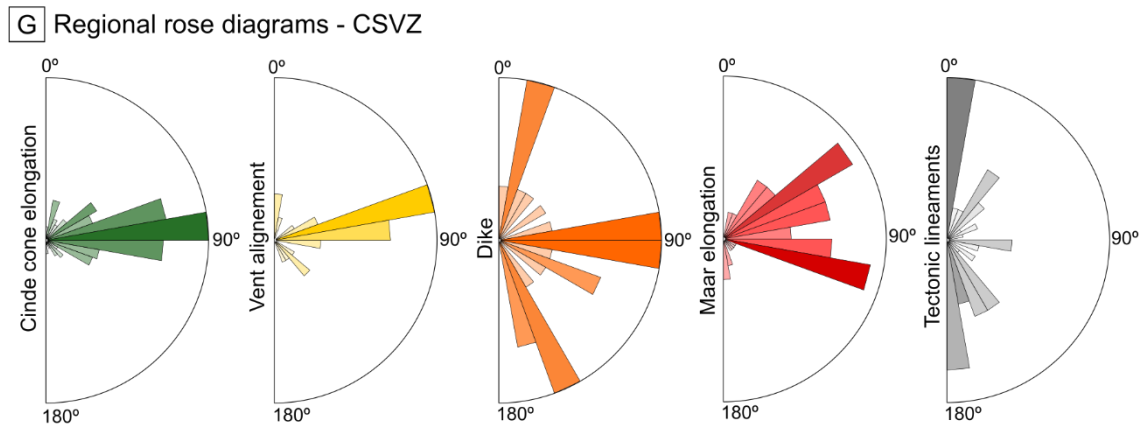
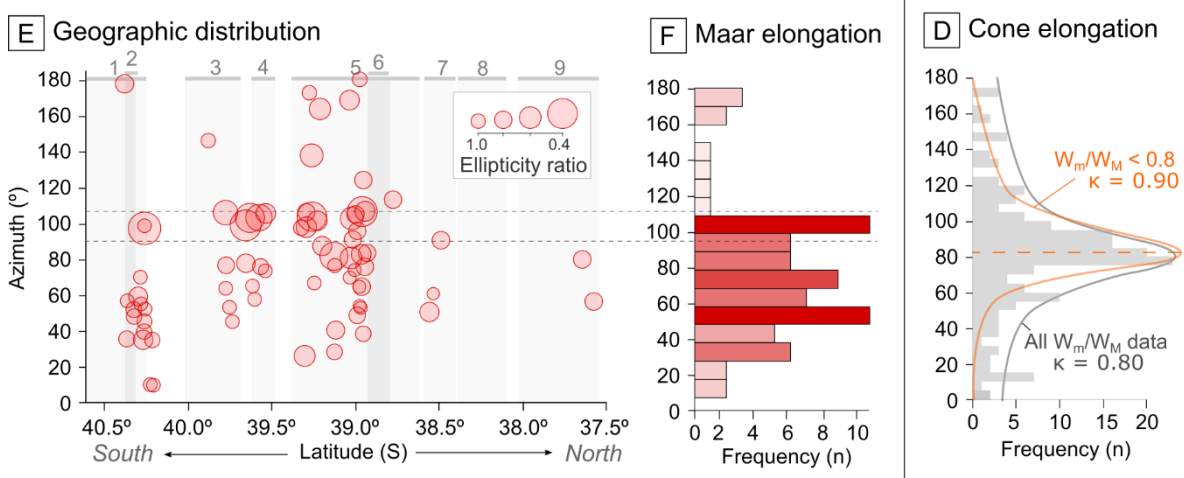
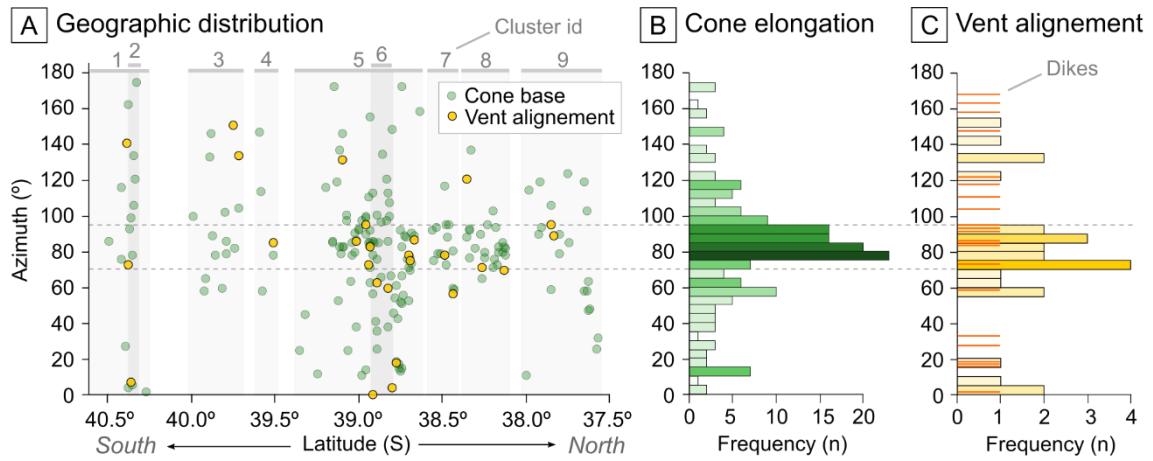
489

490

491

492

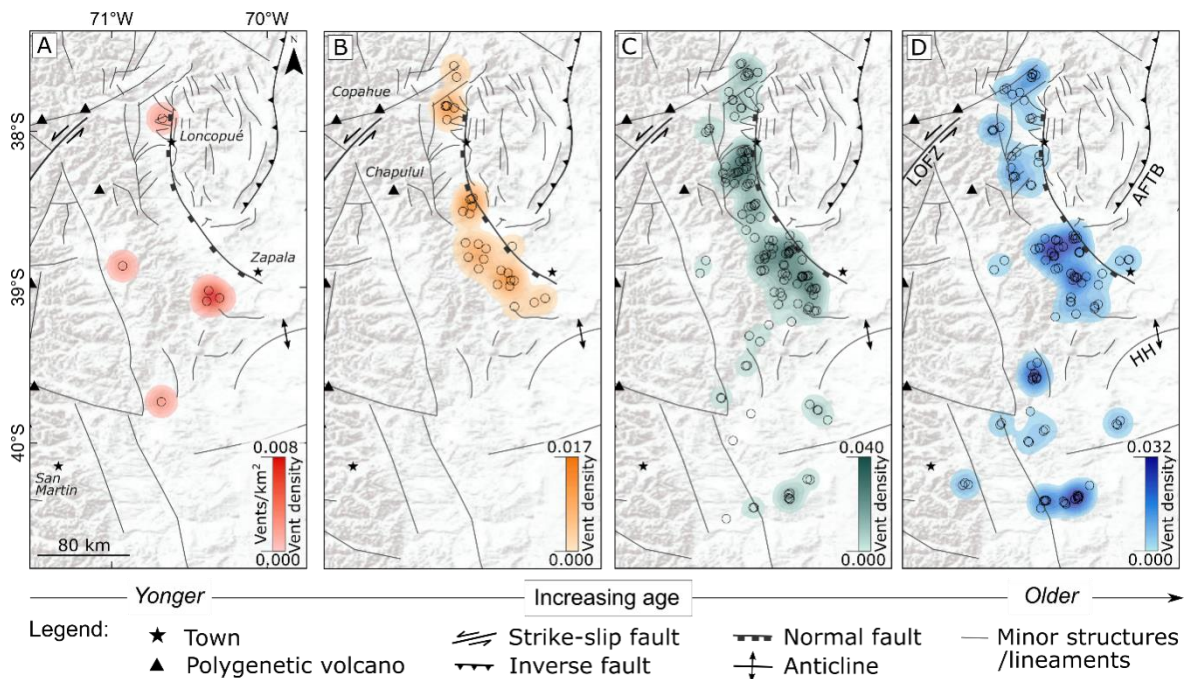
493 **Fig. 10** (below). Summary of structural analysis using monogenetic volcanoes: A) south to the north
494 geographic distribution of cinder cones basal elongation and vent alignment; B) histogram of cinder cone
495 elongation direction; C) histogram of vent alignment and dike direction, in orange; D) histogram of cinder
496 cone elongation direction taking into account all cones and only the elliptical cones ($W_m/W_M < 0.8$), κ
497 stands for kurtosis; E) south to the north geographic distribution of maar crater elongation; F) histogram of
498 maar crater elongation direction; G) regional rose diagrams form cinder cone elongation, vent alignment,
499 dikes, maar crater elongation, and the tectonic structures/lineaments; H) local rose diagrams of cinder cone
500 elongation for each monogenetic cluster within the ZVF, vent alignment directions are represented as yellow
501 dots.



503 4.4. Relative age

504 Using the relative age classification method, it was possible to map the temporal
 505 distribution of cinder cones in the ZVF. Similar to the approach used by Haag et al. (2019),
 506 we use relative ages of cinder cones to interpolate regional maps, expressing the results as
 507 density maps for each relative age class (Fig. 11A- D).

508 Our data indicate that the younger monogenetic volcanoes appear to concentrate
 509 southwest of Zapala Town (Fig. 11A), with more isolated occurrences a few kilometers
 510 northwest of Loncopué Town (Fig. 11A). Moderately young cones present a wide
 511 distribution to the eastward, apparently following an NW-SE-trending normal fault and
 512 concentrated in the Loncopué Trough (Fig. 11B).



513

514 **Fig. 11.** Density maps with the regional distribution of each relative age class: A) young; B) moderately
 515 young; C) mature; D) old. Monogenetic volcanoes are expressed by open circles. All densities are in
 516 volcanoes/km².

517 Mature landforms (moderately degraded landforms) are widespread in the study
 518 area and especially concentrate in the northwest and southwest regions of the Zapala and
 519 Loncopué Towns (Fig. 11C). These features present a similar distribution to moderately
 520 young landforms (Fig. 11B), however mature cones also occur as isolated clusters to the
 521 south of Zapala Town (Fig. 11C). Older monogenetic volcanoes are also widespread in the
 522 study area, with occurrences to the northwest of Loncopué, and next to the Chapulul

523 volcano (Fig. 11D). Several old cinder cones also occur in the north-northwest of Zapala
524 and in the extreme southwest of the study region, near the city of San Martín along the
525 Neuquén Basin (Fig. 11D).

526

527 **5. Discussion**

528 *5.1. Geomorphology and morphometry*

529 The monogenetic volcanism in the ZVF is marked by the predominance of cinder
530 cones that present a clear association with local lineaments, suggesting a structural control
531 on the occurrence of the monogenetic vents. The presence of cinder cones suggests a
532 prevalence of the strombolian style as the main eruption dynamics in the ZVF (Németh and
533 Kereszturi, 2015), similarly to the Puna Plateau in the Central Andes (Filipovich et al.,
534 2019; Haag et al., 2019; Maro and Caffè, 2016; Morfulis et al. 2020). This dynamic is
535 supported by the number of hydrovolcanic landforms in the region (less than 20%), which
536 denotes a limited, however existing, magma-water influence in the eruption history of
537 individual vents of the ZVF

538 The cinder cones present morphometric signatures (e.g., W_M , H_c) similar to
539 extension-related cones when compared to the global dataset of Fornaciai et al. (2012)
540 (Fig. 12A). These cones are marked by lower H_c/W_M ratios when compared to cinder
541 cones associated with compressional environments (Fornaciai et al., 2012).

542 The use of traditional morphometric parameters (e.g., H_c/W_M ratio) to the
543 determination of relative ages typically results in misleading interpretations (Hasenaka and
544 Carmichael, 1985; Uslular et al., 2021), because after the eruption the morphometric
545 parameters are subject to several modifications related to weathering and tectonics.
546 Furthermore, many syn-eruptive processes can produce a variety of primary landforms,
547 with extensive contrasts in H_c/W_M ratios (Kereszturi and Nemeth, 2012). In contrast,
548 alternative approaches using cone flank slope (S_{co}) and contour curves have returned valid
549 results (e.g., Inbar et al., 2011; Haag et al., 2019; Zarazúa-Carbajala and Cruz-Reyna,
550 2020). In ZVF cones, we observe a systematic decrease in S_{co} following the relative age,
551 in which young landforms tend to present higher S_{co} values when compared to the older
552 ones (Fig. 12B). Despite this general trend in average values, there is a considerable

553 deviation and scattering in the data (Fig. 12B). This scattering is likely associated with
554 contrasting initial cone morphology, mainly controlled by tectonics, terrain slope, and
555 eruption dynamics (Kervyn et al., 2012; Bemis and Ferencz, 2017; Haag et al. 2019;
556 Uslular et al., 2021).

557 Phreatomagmatic volcanoes tend to concentrate to the south of 39°S and typically
558 below 1,600 m a.s.l. (Fig. 6C), suggesting a geographic control on the occurrence of
559 hydrovolcanism in the ZVF. This distribution may be associated with the decrease of water
560 availability with increasing elevation. Using a global dataset of maar volcanoes, Sonder
561 (2018) observed a substantial decrease in the number of maar volcanoes above 2,000 m
562 a.s.l.

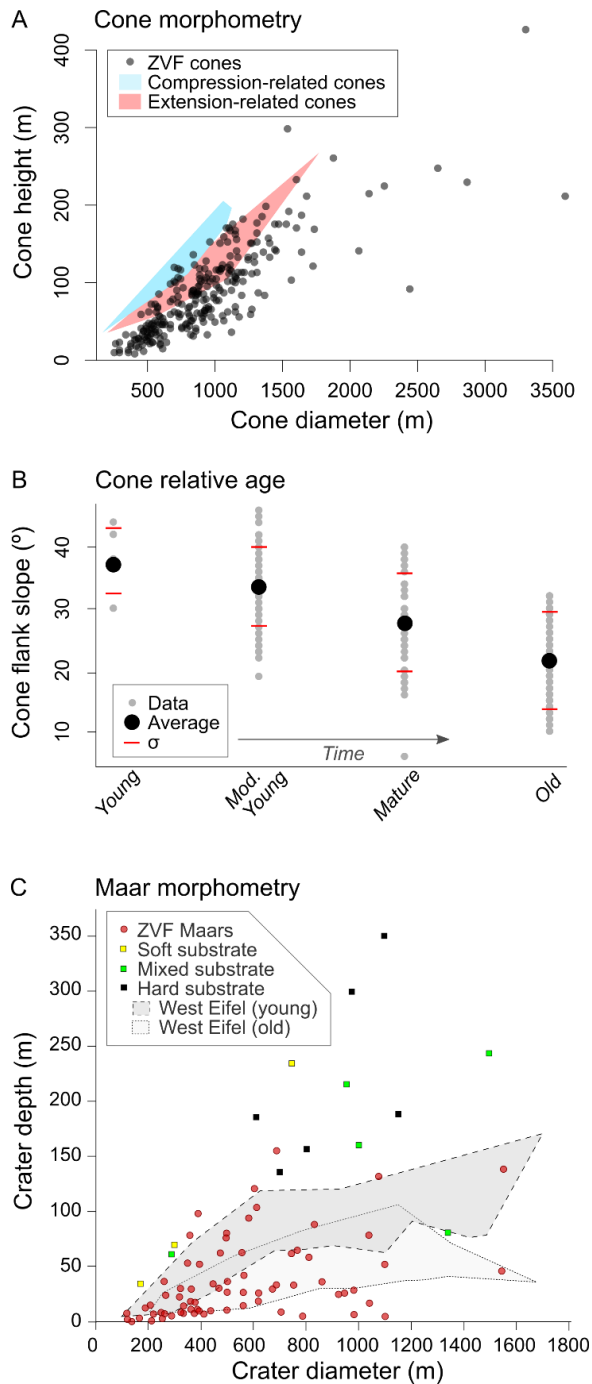
563 The sharp decrease in maar volcanoes observed in Fig. 6A and B may also be
564 associated with geological controls. Phreatomagmatic activity depends on the availability,
565 location and proportion of groundwater (Németh and Kereszturi, 2015; Ureta et al., 2021a).
566 The regional basement to the south of 39°S is marked by the presence of sedimentary
567 sequences of the Neuquén Basin, which possibly control the distribution of
568 hydrovolcanism in the ZVF (D'Elia et al., 2016).

569 In contrast to cinder cones, the original morphology and subsequent modifications
570 of maar craters are strongly controlled by substrate rheology. Ross et al. (2011) discuss
571 these factors by comparing the morphology of maar craters emplaced on hard, soft, and
572 mixed substrates in the Pali Aike Volcanic Field (Argentina). Mixed substrates are marked
573 by the presence of soft (typically of sedimentary origin) and hard (typically volcanic or
574 metamorphic) materials. Maar craters in the ZVF present variable depth/diameter ratios,
575 suggesting a predominance of mixed substrates when compared to the dataset of Ross et al.
576 (2011) (Fig. 12C). In the ZVF, maars with similar diameters but deeper craters are
577 typically emplaced on top of sedimentary sequences capped by extensive lava flows,
578 forming volcanic plateaus. In contrast, shallower maar craters are generally associated with
579 soft substrates marked by sedimentary and alluvial sequences.

580 Additionally, several ZVF maars are preceded by cinder cones, denoting a shift in
581 the eruption dynamics from strombolian to phreatomagmatic. This dynamic behavior of
582 phreatomagmatic eruptions/systems has been observed in several places around the world,
583 including hyper-arid regions such as the Atacama Desert in Chile (Ureta et al., 2021a,

584 2021b). Ultimately, phreatomagmatic activity in these regions seems to be controlled by
 585 water availability and water table depth (Ureta et al., 2021b).

586



587

588 **Fig. 12.** Morphometric comparison of monogenetic landforms presents at ZVF: A) cinder cones
 589 morphometry, modified from Fornaciai et al. (2012); σ = standard deviation; B) relative age morphometry;
 590 C) maars morphometry and its relationship with substrate styles, modified from Ross et al. (2011).

591 *5.2 Spatial distribution*

592 Monogenetic volcanoes in the ZVF present an average vent density of 0.015
593 vents/km². When compared to other monogenetic fields, the ZVF average density is higher
594 than values obtained for the Southern Puna Plateau (0.008 vents/km²; Haag et al., 2019),
595 lower than the San Rafael (0.071 vents/km², in the USA; Kiyosugi et al., 2012), and
596 significantly lower than the Auckland (0.146 vents/km², in New Zealand; Le Corvec et al.,
597 2013) and the Michoacán (0.260 vents/km², in México; Pérez-López et al., 2011) volcanic
598 fields. In contrast, the ZVF maximum vent density of 0.144 vents/km² is comparable to
599 values obtained for the Southern Puna (Haag et al., 2019; Morfulis et al., 2020). Similarly
600 to other monogenetic fields (e.g., Puna Plateau), the higher vent densities in ZVF are
601 observed in the center of the monogenetic field, in cluster 5 (Fig. 7B).

602 The interplay of tectonics and magmatism controls the distribution of monogenetic
603 volcanoes (e.g., Báez et al., 2017). The understanding of these dynamics and its surface
604 expression has been the focus of several studies (e.g., Tibaldi, 1995; Tadini et al., 2014).
605 Based on the distribution pattern of monogenetic vents in the Southern Puna Plateau,
606 Morfulis et al. (2020) suggest two styles for monogenetic volcanic fields: (I) fields
607 controlled by magmatic activity, with clustered pattern (R-statistic→0.0) and (II) field
608 controlled by tectonics, with Random and Poisson distribution pattern (R-statistic→1.0).

609 The monogenetic vents in the ZVF present three distribution patterns: clustered
610 (cluster 1, 5, and 9), Poisson distribution (clusters 3 and 8), and dispersed (cluster 2, 4, 6,
611 and 7). This complex pattern is likely related to different magma production rates through
612 the ZVF, where clusters 1, 5, and 9 would represent regions of relatively high and/or long-
613 lasting magma supply (Báez et al., 2017; Morfulis et al., 2020).

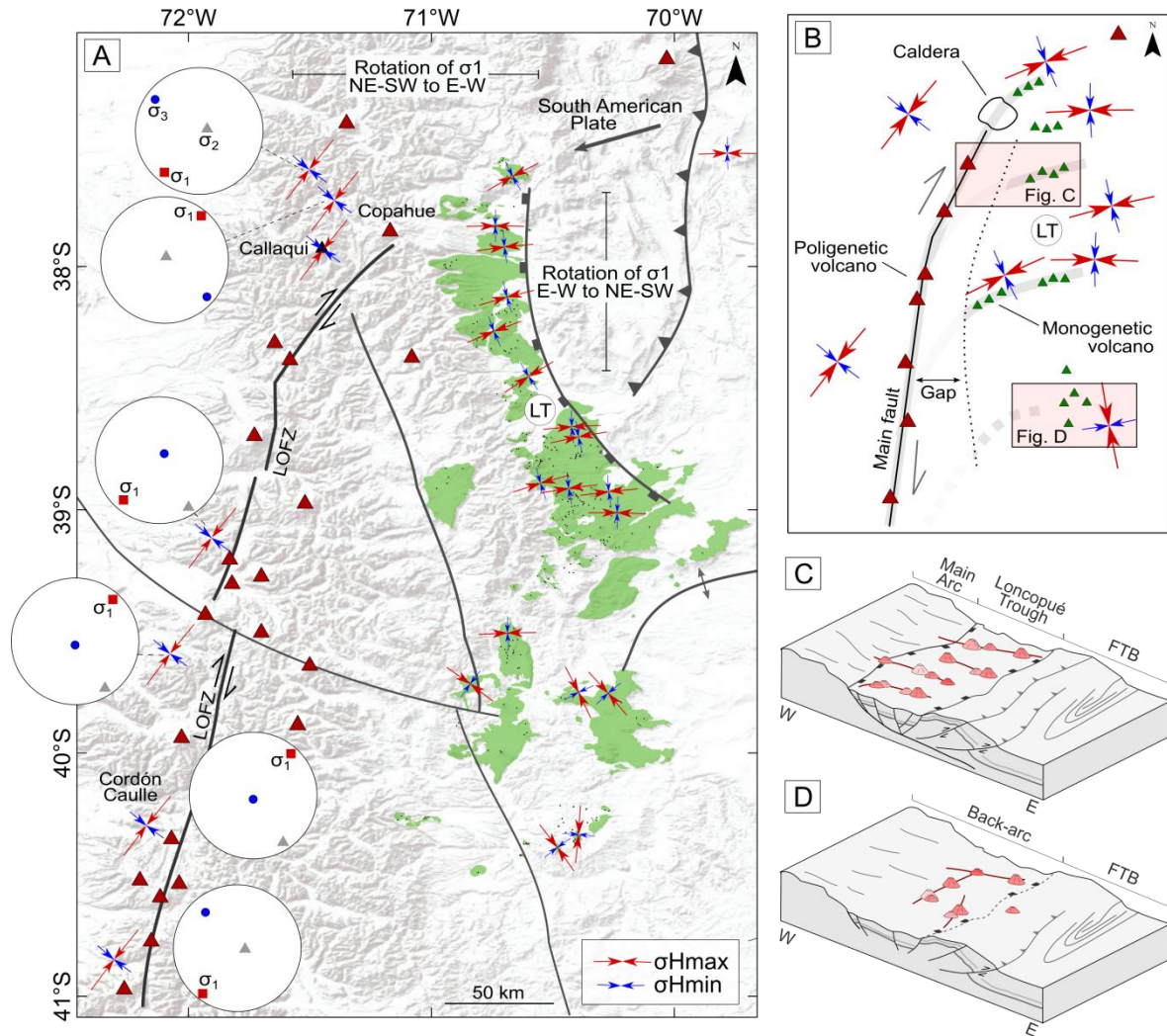
614 *5.3. Tectonic and structural implications*

615 The Southern Andes is marked by a strong oblique component in the subduction of
616 the Nazca Plate under the South American Plate (Fig. 1A; Stern, 2004). This setting offers
617 a unique opportunity to explore the interplay of volcanic systems and tectonics. The
618 oblique deformation in the Central SVZ is mainly accommodated by the 1200 km-long
619 LOFZ (Cembrano et al., 1996), which controls the distribution of polygenetic volcanoes in
620 the current volcanic arc. To date, the effects of this oblique tectonics on volcanism have
621 been explored by a few studies mainly focused on the orientation and morphology of

622 stratovolcanoes located in the magmatic arc (e.g., Lara et al., 2006; Melnick et al., 2006;
623 Sielfeld et al., 2017).

624 Cembrano and Lara (2009) identify two sets of volcanic associations in the eastern
625 (Chilean) SVZ based on volcano morphology and distribution: (1) NE-trending volcanoes
626 that reflect the current tensional regime and (2) stratovolcanoes associated with ancient
627 basement reverse and strike-slip faults and monogenetic cones along the LOFZ that
628 diverge in orientation with the current tensional regime. These observations combined with
629 structural data suggest an overall NE-SW trending maximum compressive stress (σ_1)
630 orientation at the magmatic arc (Fig. 13A; Cembrano and Lara, 2009 and references
631 therein; Melnick et al., 2006; Sielfeld et al., 2017). In contrast, studies about the
632 morphology of monogenetic volcanoes and they relate to stress state in the back-arc SVZ
633 are still scarce.

634 Based on edifice morphology and vent alignment, our data suggest that
635 monogenetic vents in the CSVZ are preferentially emplaced along NE-SW and E-W
636 trending structures (Fig. 10G). It is important to note that this result is consistent across
637 different values of basal cones ellipticity, and even better constrained when considering
638 only cones with ellipticity < 0.8 (Fig 10D). This suggests some common underlying control
639 on the emplacement of the monogenetic cones in the study area. Therefore, this orientation
640 can be used to infer the stress state (e.g., Le Corvec et al., 2013; Marliyani et al., 2020) in
641 the CSVZ back-arc region, implying a maximum horizontal compressive stress (σ_{Hmax})
642 with NE-SW to E-W direction, in agreement with Quaternary stress orientation (Cembrano
643 and Lara, 2009) (Fig. 13). The E-W orientation is also in agreement with several structures
644 that control the emplacement of lavas on the Copahue Volcano (Bonali et al., 2016).



645

646 **Fig. 13.** Tectonic model for monogenetic volcanism in the CSVZ: A) regional map with main structural
 647 features, polygenetic volcanoes, and monogenetic deposits. B) Conceptual model for the emplacement of
 648 monogenetic volcanoes in the CSVZ; C) detail of the Loncopué Trough region next to cluster 5; D) detail of
 649 the southern CSVZ. Stereoplots indicate available data from the literature (Lara et al., 2006; Melnick et al.,
 650 2006; Cembrano and Lara, 2009, Pardo et al., 2006; Lange et al., 2008; Potent and Reuther, 2001; Rosenau et
 651 al., 2004; Lavenu and Cembrano, 1999; Arancibia et al., 1999; Sielfeld et al., 2017). Legends are the same as
 652 Fig. 1. LT = Loncopué Trough, FTB = Fold and thrust belt.

653 Our data reveals that back-arc monogenetic vents seem to concentrate along
 654 secondary faults that diverge from the LOFZ (Fig. 13A), possibly because of the strong
 655 oblique component acting on the CSVZ. In transtensional environments, secondary
 656 structures can diverge from the master fault, forming imbricated fans of extensional
 657 fractures (Kim et al., 2003; Fig. 13B). To date, the occurrence of monogenetic volcanism
 658 associated with these structures has only been observed in the Wulanhada volcanic field, in
 659 Northern China, where a strike-slip dextral fault accommodates deformation and controls

660 the distribution of monogenetic volcanoes (Zhao et al., 2019). In contrast, Wulanhada
661 deposits are considerably smaller (in area) when compared to the CSVZ, with only 41
662 vents and deposits that cover $\sim 180 \text{ km}^2$ (Zhao et al., 2019).

663 Another important feature in the CSVZ is the Loncopué Trough (Rojas Vera et al.,
664 2014; Pesce et al., 2019; 2020). Located between the main volcanic arc and the Agrio Fold
665 and Thrust Belt, this 300 km long extensional structure controls the occurrence of
666 monogenetic volcanism (Rojas Vera et al., 2014; Fig. 13A, C). Inside the Loncopué
667 Trough, the monogenetic magmatism develops as continuous lava plateaus from early
668 Pliocene to present (Rojas Vera et al., 2014). Based on fieldwork and geophysical data, the
669 Loncopué Trough seems to be associated with tearing of the subducted Nazca plate
670 underneath the South American Plate, resulting in abnormal heat flow in the region (Rojas
671 Vera et al., 2014). In this scenario, monogenetic activity seems to be controlled by the
672 extensional regime at the Loncopué Trough, in addition to the oblique tectonics of the
673 LOFZ.

674 In this setting, the growth and orientation of monogenetic volcanoes can be
675 extensively controlled by transcurrent faults (e.g., Pasquarè and Tibaldi, 2003; Tibaldi and
676 Bonali, 2018; Tibaldi et al., 2017; Zhao et al., 2019). However, Pasquarè and Tibaldi
677 (2003) show that dykes are emplaced parallel to the regional σ_{Hmax} , regardless to the
678 volcano/fault proximity. This could explain why most monogenetic volcanoes in the ZVF
679 present ENE-WNW trending basalt elongations and alignment, in accordance with the
680 regional shortening induced by the Andean orogeny.

681 Monogenetic volcanoes in CSVZ also reveal changes in σ_{Hmax} direction, which
682 seem to be mainly controlled by their distance to the master LOFZ, or possibly by
683 interference secondary structural features in the Loncopué Trough and the fold and thrust
684 belt (Fig. 13A, B, C). The north end of the monogenetic field is marked by NE-SW-
685 trending σ_{Hmax} , almost parallel to σ_{Hmax} observed in the main magmatic arc (Fig. 13A).
686 This orientation is compatible with extensional faults and *horsetail splays* frequently
687 observed at the end of strike-slip structures such as the LOFZ (Kim et al., 2003). The
688 northern limit of the Loncopué Trough is marked by a significant change in the σ_{Hmax}
689 from NE-SW to the E-W (Fig. 13A). This σ_{Hmax} E-W direction progressively rotates
690 toward NE-SW as we move south in the Loncopué Trough (Fig. 13A). There is another
691 significant change in the σ_{Hmax} at ca. $38^{\circ}30'$, where σ_{Hmax} becomes E-W oriented (Fig.

692 13A). Further south in the CSVZ, σ_{Hmax} becomes less constrained and presents variable
693 orientations, including NW-SE, NNW-SSE, and N-S (Fig. 13D).

694 Changes in the stress orientation using volcano morphology have been recently
695 reported in the Java Volcanic Arc (Marliyani et al., 2020). The authors associated the
696 progressive changes in σ_{Hmax} to relative plate convergence and upper plate structure,
697 while abrupt changes are linked to the presence of preexisting structures, as well as to
698 interference of polygenetic volcanoes (Marliyani et al., 2020). Differently from Java,
699 monogenetic volcanoes in the CSVZ are predominantly located several kilometers away
700 from the main volcanic arc (Fig. 1B). In this context, the only cluster expected to suffer
701 influence from the arc is cluster 9, which presents a bimodal distribution of basal
702 elongation (Figs. 9A, 9F).

703 *5.4. Timing and recurrence of monogenetic activity*

704 Absolute ages are scarce for ZVF and mainly concentrated at $\sim 39^{\circ}S$. Most results
705 indicate quaternary ages for the monogenetic activity, although the presence of multiple
706 magmatic pulses is still unclear. Samples from the Loncopu  Trough indicate ages between
707 2.30 ± 0.3 and 0.47 ± 0.2 Ma (K-Ar whole-rock; Linares & Gonzalez 1990). Ages of
708 0.130 ± 0.02 0.167 ± 0.005 2.50 ± 5 and 809 ± 12 ka are also reported for basaltic lavas further
709 along the same structure (^{40}Ar - ^{39}Ar ; Rabassa et al., 1987; Rojas Vera et al., 2014).
710 Additional ages ranging from 1.6 ± 0.2 and 0.9 ± 0.3 Ma (K-Ar whole-rock) are also
711 reported by Mu oz & Stern (1985, 1988) for samples in the Pino Hachado region, in the
712 southernmost ZVF.

713 In this scenario of scarce absolute ages, relative age maps offer an alternative
714 method for mapping the monogenetic activity through time (e.g., Haag et al., 2019). The
715 interpolated relative age maps (Fig. 11) suggest a waning monogenetic activity in the ZVF
716 over time: while the older monogenetic volcanoes are widespread in the ZVF (Fig. 11D),
717 the younger landforms seem to be focused in the central segment of the volcanic field (Fig.
718 11A), near to the Zapala and Loncopu  towns.

719 Geological mapping and fieldwork in the study area also suggest multiple episodes
720 of monogenetic activity in the region (Rojas Vera et al., 2014; Pesce et al., 2019).
721 Intercalated basaltic flows and glacial deposits are reported along the Loncopu  trough
722 (Folguera et al., 2003b), suggesting at least two magmatic pulses in the region. Additional

723 mapping by Báez et al., (2020) in the Caviahue-Copahue Volcanic Complex indicates the
724 occurrence of at least two glaciations in the region (at 57-29 ka and/or 26.5-19.0 ka and at
725 14.5-11.9 ka). The 809 Ka basaltic flows are incised by a glacial valley in the western
726 Loncopué Trough (Rojas Vera et al., 2014). These glacial valleys also control
727 emplacement of younger, post-glacial activity with estimated ages to be less than 27 ka
728 (Rojas Vera et al., 2014).

729 Monogenetic eruptions can be triggered by several factors because of their shallow
730 magma chambers. Bonali et al. (2013) report stress changes induced by earthquakes in the
731 SVZ. In the area, several earthquake-induced eruptions can occur as far as 500 km from
732 the epicenters (Bonali et al., 2013). This finding highlights the role of earthquakes in
733 inducing monogenetic activity, specially in subduction zones such as the SVZ.

734 The predominance of E-W and NE-SW feeding systems in the CSVZ is at odds
735 with the regime responsible for the development of the Loncopué Trough, which is mainly
736 associated with N-S normal faults developed under a E-W extension (Rojas Vera et al.,
737 2014). This information suggests a decoupling between the stress state recorded by
738 monogenetic feeding systems and the structural setting at the Loncopué Trough. Curiously,
739 numerous N-S trending normal faults cut the monogenetic deposits to the east of Caviahue
740 and next to the Loncopué Town (Rojas Vera et al., 2014; Pesce et al., 2019), suggesting
741 ongoing deformation of the quaternary monogenetic volcanism.

742 *5.5. Comparison with monogenetic fields in the Central Andes*

743 For a long time, the study of monogenetic volcanoes has been hampered by the
744 coarse resolution of DEMs and imagery data. Therefore, a greater focus has been placed on
745 the study of large, polygenetic volcanoes. However, in recent years, the available high-
746 resolution DEMs allowed the identification of thousands of monogenetic volcanoes in the
747 Andean Cordillera.

748 Most of these studies have been focused in the Central Volcanic Zone of the Andes
749 (CVZ; 18-28° S; e.g., Maro and Caffè, 2016; Tibaldi et al., 2017; Tibaldi and Bonali, 2018;
750 Filipovich et al., 2019; Haag et al., 2019; Grosse et al., 2020; Morfulis et al., 2020; Ureta et
751 al., 2021c). In contrast, studies involving geomorphologic characterization of monogenetic
752 volcanoes in the Southern Volcanic Zone (SVZ) of the Andes are still scarce. In this
753 section, we compare our results obtained at the ZVF (in the Central SVZ) with the

754 available data for the CVZ (mainly for the southern Puna Plateau). A summary of this
755 comparison is presented in Table 2.

756 Monogenetic volcanoes in the ZVF present a higher number of phreatomagmatic
757 volcanoes (20%) when compared to other monogenetic fields in the Andes, such as the
758 southern Puna Plateau (Haag et al., 2019). This difference could be attributed to climate
759 variations between these regions: while the ZVF is marked by a wet climate with the
760 presence of lakes and vegetation, the Puna Plateau sits above 3 km and comprises one of
761 the aridest regions on Earth. The presence of sedimentary rocks of the Neuquén Basin as
762 underlying units in the ZVF may also contribute to the occurrence of phreatomagmatism.
763 In contrast, overlying units in the southern Puna Plateau are mainly metamorphic and
764 igneous rocks (Schnurr et al., 2006, Seggiaro et al., 2006).

765 Another important fact to be considered is the absence of lava domes in the ZVF.
766 Conversely, flat-topped and irregular lava domes are expressive and widespread
767 monogenetic landforms in the southern Puna Plateau (Haag et al., 2019), as well as in the
768 entire CVZ of the Andes (Ureta et al., 2021). We interpret this absence of lava domes in
769 the CSVZ as a result of contrasting melt compositions and evolution in these two areas.
770 Magmas associated with the ZVF are mainly basalts with arc to back-arc signatures
771 (Varekamp et al., 2010; Rojas Veras et al., 2014). In contrast, the monogenetic volcanism
772 in southern Puna Plateau includes more evolved terms, such as basaltic-andesites and
773 andesites.

774 In this scenario, the presence of lava domes may reflect contrasting petrogenetic
775 conditions in the CVZ and SVZ: while the southern Puna is marked by crustal thickness of
776 ~70 km (Trumbull, et al., 2006), the ZVF crust is considerably thinner, ranging from 30 to
777 35 km (Munizaga et al., 1988; Nelson et al., 1993; Stern 2004), yielding less evolved
778 magmas and the absence of lava domes.

779

780

781

782

783 **Table 2.** Comparison of monogenetic volcanism in the SVZ and the CVZ of the Andes.

Parameters	Region of the Andes	
	South (Central SVZ at ZVF)	Central (Southern Puna Plateau)
Edifice morphology	80 % Cinder Cones 20% Pheatomagmatic 0% Domes	76% Cinder Cones 15% Domos 7% Pheatomagmatic (Haag et al., 2019)
Cone diameter - Wco (m)	246 to 3590	200 to 3800 (Haag et al., 2019)
Cone height- Hco (m)	7 to 426	2 to 308 (Haag et al., 2019)
Average vent density (vents /km ²)	0.015	0.0083 (Haag et al., 2019)
Maximum vent density (vents /km ²)	0.144	0.149 to 0.237 (Haag et al., 2019, Morfulis et al., 2020)
Exogenous controls - climate	Dry and wet	Predominately dry (Filipovich et al., 2019; Haag et al., 2019)
Subduction style and regional σ_1	Oblique, NE-SW (Lara et al., 2006 and references therein)	Almost orthogonal, NW-SE (Marrett and Emerman, 1992)
Vent alignment	E-W to ENE-WSW (primary) and N-S (reactivated?)	NNE-SSW (reactivated); NW-SE (normal; strike-slip) (Haag et al., 2019)
Monogenetic magmatism	Waning	Waxing (Haag et al., 2019)
Crustal thickness	30- 35 Km (Munizaga et al., 1988; Nelson et al., 1993; Stern, 2004)	~ 70 Km (Trumbull et al., 2006)
Geochemical origin	Arc to back-arc (Varekamp et al., 2010; Rojas Vera et al., 2014)	Lithospheric delamination (Kay and Kay, 1993) and foundering (Schoenbohm and Carrapa, 2015)
Age	2.3 Ma - Recent (Linares & Gonzalez 1990; Rabassa et al., 1987; Muñoz & Stern 1985, 1988)	9.0 Ma - Recent (Risse et al., 2008; Drew et al., 2009; Schoenbohm and Carrapa, 2015)

784

785

786

787

788 **6. Conclusions**

789 In this work, we combine imagery and digital elevation models to map the
790 occurrence of monogenetic volcanoes in the back-arc region of the Central Southern
791 Volcanic Zone (CSVZ) of the Andes. The main conclusions are:

792 1. The CSVZ presents a predominance of cinder cones (80%) followed by a
793 significant number of phreatomagmatic volcanoes (20%). This data implies the
794 strombolian as the main eruption style but also reveals an important role of water and
795 hydromagmatism in the eruption dynamics of monogenetic vents. The occurrence of
796 phreatomagmatism is either associated with climate (elevations below 1.600 m a.s.l.) or
797 geological controls (basement porosity and water availability).

798 2. Monogenetic volcanoes are grouped into nine clusters. The higher vent densities
799 are observed in the center of the CSVZ to the south of the Loncopué Though. Each cluster
800 is marked by contrasting vent distribution and organization that reflect the interplay of
801 tectonics and magmatism (e.g., Báez et al., 2017; Morfulis et al., 2020).

802 3. Monogenetic vents show a clear association with local and regional lineaments,
803 suggesting a strong structural control on the occurrence of monogenetic deposits. The main
804 controls on the distribution of monogenetic vents are the oblique tectonics of the Liquiñe-
805 Ofqui Fault Zone and the extensional Loncopué Though.

806 4. Based on edifice morphology and distribution, monogenetic volcanoes are
807 preferentially emplaced along NE- SW and E-W trending structures that reflect the stress
808 state in the CSVZ (e.g., Le Corvec et al., 2013; Marliyani et al., 2020).

809 5. With scarce absolute ages for the region, relative age offers an alternative
810 approach to map monogenetic activity over time. This data suggests a decrease in the aerial
811 extend of monogenetic activity in the CSVZ.

812 6. When compared to monogenetic deposits in the Central Andes, the Southern
813 Andes are defined by higher vent densities, a higher number of phreatomagmatic
814 landforms, and the absence of lava domes. This likely reflects climate and crustal structure
815 differences of these two regions.

816

817 **Acknowledgments**

818 This article is part of F.S.S. PhD's thesis at Geosciences Institute at Universidade Federal
819 do Rio Grande do Sul, sponsored by the Conselho Nacional de Desenvolvimento Científico
820 e Tecnológico of Brazil. F.S.S thanks Coordenação de Aperfeiçoamento de Pessoal de
821 Nível Superior (CAPES, Brazil) for the financial support. Carlos A. Sommer thanks Conselho
822 Nacional de Desenvolvimento Científico e Tecnológico (CNPq, Brazil) for the research grant and
823 financial support (305036/2018-8, 406825/2018-6). The authors are grateful to reviews of Károly
824 Németh and two anonymous reviewers who provided important suggestions to improvement of the
825 manuscript.

826

827 **References**

- 828 Arancibia G., Cembrano J., Lavenu A. 1999., Transpresión dextral y partición de la
829 deformación en la Zona de Falla Liquiñe- Ofqui, Aisén, Chile (44- 45°S) *Revista*
830 *Geológica de Chile*, 26 (1), pp. 3-22.
- 831 Báez, W., Carrasco Nuñez, G., Giordano, G., Viramonte, J.G., Chiodi, A., 2017. Polycyclic
832 scoria cones of the Antofagasta de la Sierra basin, Southern Puna plateau, Argentina.
833 *Geological Society, London, Special Publications* 446, 311–336.
834 <https://doi.org/10.1144/sp446.3>
- 835 Báez, A.D., Báez, W., Caselli, A.T., Martini, M.A., Sommer, C.A., 2020. The
836 glaciovolcanic evolution of the Copahue volcano, Andean Southern Volcanic Zone,
837 Argentina-Chile. *Journal of Volcanology and Geothermal Research* 396, 106866.
838 <https://doi.org/10.1016/j.jvolgeores.2020.106866>
- 839 Barreiro, B. A., 1984. Lead isotopes and Andean magma genesis. In *Andean magmatism:*
840 *chemical and isotopic constraints*. Shiva Geology Series, Shiva Publishing Limited,
841 Natwich, UK 21-39.
- 842 Bemis, K.G., Ferencz, M., 2017. Morphometric analysis of scoria cones: the potential for
843 inferring process from shape. *Geological Society London* 446 (1), 61–100.
844 <https://doi.org/10.1144/SP446.9>.

- 845 Bishop, M.A., 2007. Point pattern analysis of eruption points for the Mount Gambier
846 volcanic sub-province: a quantitative geographical approach to the understanding of
847 volcano distribution. *Area* 39, 230–241. <https://doi.org/10.1111/j.1475-4762.2007.00729.x>
- 848 Bonali, F.L., Corazzato, C., Tibaldi, A., 2011. Identifying rift zones on volcanoes: an
849 example from La Réunion island, Indian Ocean. *Bull Volcanol.*
850 <https://doi.org/10.1007/s00445-010-0416-1>
- 851 Bonali, F.L., Tibaldi, A., Corazzato, C., Tormey, D.R., Lara, L.E., 2013. Quantifying the
852 effect of large earthquakes in promoting eruptions due to stress changes on magma
853 pathway: The Chile case. *Tectonophysics*. <https://doi.org/10.1016/j.tecto.2012.10.025>
- 854 Bonali, F.L., Corazzato, C., Bellotti, F., Gropelli, G., 2016. Active Tectonics and Its
855 Interactions with Copahue Volcano. *Active Volcanoes of the World.*
856 https://doi.org/10.1007/978-3-662-48005-2_2
- 857 Bruno, B.C., 2004. Clustering within rootless cone groups on Iceland and Mars: Effect of
858 nonrandom processes. *J. Geophys. Res.* 109. <https://doi.org/10.1029/2004je002273>
- 859 Bruno, B.C., Fagents, S.A., Hamilton, C.W., Burr, D.M., Baloga, S.M., 2006.
860 Identification of volcanic rootless cones, ice mounds, and impact craters on Earth and
861 Mars: Using spatial distribution as a remote sensing tool. *J. Geophys. Res.* 111.
862 <https://doi.org/10.1029/2005je002510>
- 863 Cañón- Tapia, E., 2016. Reappraisal of the significance of volcanic fields. *Journal of*
864 *Volcanology and Geothermal Research* 310, 26–38.
865 <https://doi.org/10.1016/j.jvolgeores.2015.11.010>
- 866 Carbone, O., Franzese, J., Limeres, M., Delpino, D., & Martínez., 2011. El Ciclo
867 Precuyano (Triásico Tardío- Jurásico Temprano) en la Cuenca Neuquina. *Geología Y*
868 *Recursos Naturales de la Provincia del Neuquén*. Asociación Geológica Argentina, Buenos
869 Aires, 63-75.
- 870 Cebriá, J.M., Martiny, B.M., López-Ruiz, J., Morán-Zenteno, D.J., 2011. The Parícutin
871 calc-alkaline lavas: New geochemical and petrogenetic modelling constraints on the crustal
872 assimilation process. *Journal of Volcanology and Geothermal Research.*
873 <https://doi.org/10.1016/j.jvolgeores.2010.11.011>

- 874 Cembrano, J., Hervé, F., Lavenu, A., 1996. The Liquiñe Ofqui fault zone: a long-lived
875 intra-arc fault system in southern Chile. *Tectonophysics* 259, 55–66.
876 [https://doi.org/10.1016/0040-1951\(95\)00066-6](https://doi.org/10.1016/0040-1951(95)00066-6)
- 877 Cembrano, J., Lara, L., 2009. The link between volcanism and tectonics in the southern
878 volcanic zone of the Chilean Andes: A review. *Tectonophysics* 471, 96–113.
879 <https://doi.org/10.1016/j.tecto.2009.02.038>
- 880 Cordani, U. G., Ramos, V. A., Fraga, L.M., Cegarra, M., Delgado, I., de Souza, K. G.,
881 Gomes, F.E. M. & Schobbenhaus, C. 2016. Tectonic Map of South America. Scale 1: 5000
882 000. 2nd Paris: CGMW- Servicio Geológico Minero Argentino (SEGEMAR).
- 883 Cucchi, R. J., Leanza, Espejo, P.M., & González, R., 1998. Hoja Geológica 4169-I Piedra
884 del Águila. Servicio Geológico Minero Argentino (SEGEMAR) Boletín N° 242, 74.
- 885 Cucchi, R.J., Leanza, H., Repol, D., Escosteguy, L.D., González, R., Danieli, J.C., &
886 Franchi, M., 2005. Hoja geológica 3972- IV Junín de los Andes. Servicio Geológico
887 Minero Argentino (SEGEMAR) Boletín N° 357, 102.
- 888 D'Elia, L., Martí, J., Muravchik, M., Bilmes, A., Franzese, J.R., 2016. Impact of volcanism
889 on the sedimentary record of the Neuquén rift basin, Argentina: towards a cause and effect
890 model. *Basin Res* 30, 311–335. <https://doi.org/10.1111/bre.12222>
- 891 Di Traglia, F., Morelli, S., Casagli, N., Garduño- Monroy, V., 2014. Semi- automatic
892 delimitation of volcanic edifice boundaries: validation and application to the cinder cones
893 of the Tancitaro- Nueva Italia region (Michoacán- Guanajuato Volcanic Field, Mexico)
894 *Geomorphology* 219, 152-160. <https://doi.org/10.1016/j.geomorph.2014.05.002>.
- 895 Drew, S.T., Ducea, M.N., Schoenbohm, L.M., 2009. Mafic volcanism on the Puna Plateau,
896 NW Argentina: Implications for lithospheric composition and evolution with an emphasis
897 on lithospheric foundering. *Lithosphere* 1, 305–318. <https://doi.org/10.1130/154.1>
- 898 Escosteguy, L., & Franchi, M., 2010. Estratigrafía de la región de Chapelco, provincia del
899 Neuquén. *Revista de la Asociación Geológica Argentina*, 66(3), 418-429.
- 900 Escosteguy, L., Geuna, S., Franchi, M., Gonzalez Díaz, E.F., & Dal Molin, C., 2013. Hoja
901 Geológica 4172-II San Martín de los Andes. Servicio Geológico Minero Argentino
902 (SEGEMAR) Boletín N° 409, 92.

- 903 Filipovich, R., Báez, W., Bustos, E., Villagrán, A., Chiodi, A., Viramonte, J.G., 2019.
904 Eruptivestyles related to the monogenetic mafic volcanism of Pasto Ventura region,
905 SouthernPuna, Argentina. *Andean Geol.* 46 (2), 300–335.
- 906 Folguera, A., Ramos, V. A & Melnick, D., 2003b. Recurrencia en el desarrollo de cuencas
907 de intraarco, Cordillera Neuquina (37°30'). *Revista de la Asociación Geológica Argentina*,
908 58, 3-19.
- 909 Folguera, A., Zapata, T., Ramos, V.A., 2006. Late Cenozoic extension and the evolution of
910 the Neuquén Andes, in: *Evolution of an Andean Margin: A Tectonic and Magmatic View*
911 *from the Andes to the Neuquén Basin (35°-39°S Lat)*. Geological Society of America.
912 [https://doi.org/10.1130/2006.2407\(12\)](https://doi.org/10.1130/2006.2407(12))
- 913 Folguera, A., Rojas Vera, E., Bottesi, G., Zamora Valcarce, G., Ramos, V.A., 2010. The
914 Loncopué Trough: A Cenozoic basin produced by extension in the southern Central Andes.
915 *Journal of Geodynamics* 49, 287–295. <https://doi.org/10.1016/j.jog.2010.01.009>
- 916 Folguera, A., Spagnuolo, M., Vera, E.R., Litvak, V., Orts, D., & Ramos, V., 2011.
917 Magmatismo Neógeno y Cuaternario. In *Geología y Recursos Naturales De La Provincia*
918 *de Neuquén: XVIII Congreso Geológico Argentino* 275-286.
- 919 Fornaciai, A., Favalli, M cones, and their relation to geodynamic setting: A DEM-based
920 analysis. *Journal of Volcanol.*, Karátson, D., Tarquini, S., Boschi, E., 2012. Morphometry
921 of scoriaogy and Geothermal Research 217–218, 56–72.
922 <https://doi.org/10.1016/j.jvolgeores.2011.12.012>
- 923 Franzese, J.R., Spalletti, L.A., 2001. Late Triassic–early Jurassic continental extension in
924 southwestern Gondwana: tectonic segmentation and pre-break-up rifting. *Journal of South*
925 *American Earth Sciences* 14, 257–270. [https://doi.org/10.1016/s0895-9811\(01\)00029-3](https://doi.org/10.1016/s0895-9811(01)00029-3)
- 926 Franzese, J., Spalletti, L., Pérez, I.G., Macdonald, D., 2003. Tectonic and
927 paleoenvironmental evolution of Mesozoic sedimentary basins along the Andean foothills
928 of Argentina (32°–54°S). *Journal of South American Earth Sciences* 16, 81–90.
929 [https://doi.org/10.1016/s0895-9811\(03\)00020-8](https://doi.org/10.1016/s0895-9811(03)00020-8)
- 930 Gianni, G.M., Dávila, F.M., Echaurren, A., Fennell, L., Tobal, J., Navarrete, C., Quezada,
931 P., Folguera, A., Giménez, M., 2018. A geodynamic model linking Cretaceous orogeny,

- 932 arc migration, foreland dynamic subsidence and marine ingression in southern South
933 America. *Earth-Science Reviews* 185, 437–462.
934 <https://doi.org/10.1016/j.earscirev.2018.06.016>
- 935 Graettinger, A.H., 2018. Trends in maar crater size and shape using the global Maar
936 Volcano Location and Shape (MaarVLS) database. *Journal of Volcanology and*
937 *Geothermal Research* 357, 1–13. <https://doi.org/10.1016/j.jvolgeores.2018.04.002>
- 938 Groeber, P., 1928. Traslado del vulcanismo de la falda oriental de la cordillera hacia la
939 ladera occidental. *Anales de la Sociedad Argentina de Estudios Geográficos* 3(1): 210-218.
- 940 Grosse, P., Ochi Ramacciotti, M.L., Escalante Fochi, F., Guzmán, S., Orihashi, Y.,
941 Sumino, H., 2020. Geomorphology, morphometry, spatial distribution and ages of mafic
942 monogenetic volcanoes of the Peinado and Incahuasi fields, southernmost Central Volcanic
943 Zone of the Andes. *Journal of Volcanology and Geothermal Research* 401, 106966.
944 <https://doi.org/10.1016/j.jvolgeores.2020.106966>
- 945 Haag, M.B., Báez, W.A., Sommer, C.A., Arnosio, J.M., Filipovich, R.E., 2019.
946 Geomorphology and spatial distribution of monogenetic volcanoes in the southern Puna
947 Plateau (NW Argentina). *Geomorphology* 342, 196–209.
948 <https://doi.org/10.1016/j.geomorph.2019.06.008>
- 949 Hasenaka, T.E., Carmichael, I.S.E., 1985. A compilation of location, size, and geomorpho-
950 logical parameters of volcanoes of the Michoacan-Guanajuato volcanic field, central
951 Mexico: *Geofisica Internacional*, 24,577-607.
- 952 Hickey, R.L., Gerlach, D.C., Frey, F.A., 1984. Geochemical Variations in Volcanic Rocks
953 from Central-south Chile (33–42°S), in: *Andean Magmatism*. Birkhäuser Boston, pp. 72–
954 95. https://doi.org/10.1007/978-1-4684-7335-3_6
- 955 Hickey, R.L., Frey, F.A., Gerlach, D.C., Lopez-Escobar, L., 1986. Multiple sources for
956 basaltic arc rocks from the southern volcanic zone of the Andes (34°–41°S): Trace element
957 and isotopic evidence for contributions from subducted oceanic crust, mantle, and
958 continental crust. *J. Geophys. Res.* 91, 5963. <https://doi.org/10.1029/jb091ib06p05963>
- 959 Hickey -Vargas, R., Roa, H.M., Escobar, L.L., Frey, F.A., 1989. Geochemical variations in
960 Andean basaltic and silicic lavas from the Villarrica-Lanin volcanic chain (39.5 S): an

- 961 evaluation of source heterogeneity, fractional crystallization and crustal assimilation.
962 *Contributions Mineralogy Petrology*. 103, 361–386. <https://doi.org/10.1007/bf00402922>
- 963 Hickey-Vargas, R., Sun, M., López-Escobar, L., Moreno-Roa, H., Reagan, M.K., Morris,
964 J.D., Ryan, J.G., 2002. Multiple subduction components in the mantle wedge: Evidence
965 from eruptive centers in the Central Southern volcanic zone, Chile. *Geology* 30, 199.
966 [https://doi.org/10.1130/0091-7613\(2002\)030](https://doi.org/10.1130/0091-7613(2002)030)
- 967 Hooper, D.M., Sheridan, M.F., 1998. Computer-simulation models of scoria cone
968 degradation. *Journal of Volcanology and Geothermal Research* 83, 241–267.
969 [https://doi.org/10.1016/s0377-0273\(98\)00031-6](https://doi.org/10.1016/s0377-0273(98)00031-6)
- 970 Howell, J.A., Schwarz, E., Spalletti, L.A., Veiga, G.D., 2005. The Neuquén Basin: an
971 overview. *Geological Society, London, Special Publications* 252, 1–14.
972 <https://doi.org/10.1144/gsl.sp.2005.252.01.01>
- 973 Inbar, M., Gilichinsky, M., Melekestsev, I., Melnikov, D., Zaretskaya, N., 2011.
974 Morphometric and morphological development of Holocene cinder cones: A field and
975 remote sensing study in the Tolbachik volcanic field, Kamchatka. *Journal of Volcanology*
976 *and Geothermal Research* 201, 301–311. <https://doi.org/10.1016/j.jvolgeores.2010.07.013>
- 977 Kay, R.W., Mahlburg Kay, S., 1993. Delamination and delamination magmatism.
978 *Tectonophysics* 219, 177–189. [https://doi.org/10.1016/0040-1951\(93\)90295-u](https://doi.org/10.1016/0040-1951(93)90295-u)
- 979 Kay, S.M., Ardolino, A.A., Gorring, M.L., Ramos, V.A., 2006. The Somuncura Large
980 Igneous Province in Patagonia: Interaction of a Transient Mantle Thermal Anomaly with a
981 Subducting Slab. *Journal of Petrology* 48, 43–77. <https://doi.org/10.1093/petrology/egl053>
- 982 Kereszturi, G., Németh, K., 2012a. Monogenetic Basaltic Volcanoes: Genetic
983 Classification, Growth, Geomorphology and Degradation, in: *Updates in Volcanology -*
984 *New Advances in Understanding Volcanic Systems*. InTech. <https://doi.org/10.5772/51387>
- 985 Kereszturi, G., Németh, K., 2012b. Structural and morphometric irregularities of eroded
986 Pliocene scoria cones at the Bakony–Balaton Highland Volcanic Field, Hungary.
987 *Geomorphology* 136, 45–58. <https://doi.org/10.1016/j.geomorph.2011.08.005>

- 988 Kervyn, M., Ernst, G.G.J., Carracedo, J.-C., Jacobs, P., 2012. Geomorphometric variability
989 of “monogenetic” volcanic cones: evidence from Mauna Kea, Lanzarote and experimental
990 cones. *Geomorphology* 136 (1), 59–75. <https://doi.org/10.1016/j.geomorph.2011.04.009>.
- 991 Kim, Y.-S., Peacock, D.C.P., Sanderson, D.J., 2003. Mesoscale strike-slip faults and
992 damage zones at Marsalforn, Gozo Island, Malta. *Journal of Structural Geology* 25, 793–
993 812. [https://doi.org/10.1016/s0191-8141\(02\)00200-6](https://doi.org/10.1016/s0191-8141(02)00200-6)
- 994 Kiyosugi, K., Connor, C.B., Wetmore, P.H., Ferwerda, B.P., Germa, A.M., Connor, L.J.,
995 Hintz, A.R., 2012. Relationship between dike and volcanic conduit distribution in a highly
996 eroded monogenetic volcanic field: San Rafael, Utah, USA. *Geology* 40, 695–698.
997 <https://doi.org/10.1130/g33074.1>
- 998 Lange, D., Cembrano, J., Rietbrock, A., Haberland, C., Dahm, T., Bataille, K., 2008. First
999 seismic record for intra-arc strike-slip tectonics along the Liquiñe-Ofqui fault zone at the
1000 obliquely convergent plate margin of the southern Andes. *Tectonophysics* 455, 14–24.
1001 <https://doi.org/10.1016/j.tecto.2008.04.014>
- 1002 Lara, L.E., Lavenu, A., Cembrano, J., Rodríguez, C., 2006. Structural controls of
1003 volcanism in transversal chains: Resheared faults and neotectonics in the Cordón Caulle–
1004 Puyehue area (40.5°S), Southern Andes. *Journal of Volcanology and Geothermal Research*
1005 158, 70–86. <https://doi.org/10.1016/j.jvolgeores.2006.04.017>
- 1006 Lavenu, A., Cembrano, J., 1999. Compressional- and transpressional-stress pattern for
1007 Pliocene and Quaternary brittle deformation in fore arc and intra-arc zones (Andes of
1008 Central and Southern Chile). *Journal of Structural Geology* 21, 1669–1691.
1009 [https://doi.org/10.1016/s0191-8141\(99\)00111-x](https://doi.org/10.1016/s0191-8141(99)00111-x)
- 1010 Leanza, H.A., Hugo, C. A., Herrero, J. C., Donnari, E. I., and Pucci, J. C., 1997. Hoja
1011 geológica 3969- III Picun Leufú. Servicio Geológico Minero Argentino (SEGEMAR)
1012 Boletín N° 218, 135.
- 1013 Le Corvec, N., Spörli, K.B., Rowland, J., Lindsay, J., 2013. Spatial distribution and
1014 alignments of volcanic centers: Clues to the formation of monogenetic volcanic fields.
1015 *Earth-Science Reviews* 124, 96–114. <https://doi.org/10.1016/j.earscirev.2013.05.005>

- 1016 Lesti, C., Giordano, G., Salvini, F., Cas, R., 2008. Volcano tectonic setting of the
1017 intraplate, Pliocene-Holocene, Newer Volcanic Province (southeast Australia): Role of
1018 crustal fracture zones. *Journal of Geophysical Research* 113.
1019 <https://doi.org/10.1029/2007jb005110>
- 1020 Llambías, E. J., & Rapela, C.W., 1989. Las volcanitas de Collipulli, Neuquén (37S) y su
1021 relación con otras unidades paleógenas de la cordillera. *Revista de la Asociación Geológica*
1022 *Argentina*, 44 (1-4), 224-236.
- 1023 Linares E., & Gonzalez, R.R., 1990. Catálogo de edades radiométricas de la República
1024 Argentina 1957-1987. Asociación Geológica Argentina, Publicaciones Especiales Série B,
1025 Didáctica y Complementaria, 19- 1- 628.
- 1026 Macfarlane, A.W., 1999. Isotopic studies of northern Andean crustal evolution and ore
1027 metal sources, In *Geology and Ore Deposits of the Central Andes* (Skinner, B.J. editor).
1028 *Society of Economic Geologists* 7, 195-217.
- 1029 Marliyani, G.I., Helmi, H., Arrowsmith, J.R., Clarke, A., 2020. Volcano morphology as an
1030 indicator of stress orientation in the Java Volcanic Arc, Indonesia. *Journal of Volcanology*
1031 *and Geothermal Research* 400, 106912. <https://doi.org/10.1016/j.jvolgeores.2020.106912>
- 1032 Maro, G., Caffè, P.J., 2016. Neogene monogenetic volcanism from the Northern Puna
1033 region: products and eruptive styles. *Geological Society, London, Special Publications*
1034 446, 337–359. <https://doi.org/10.1144/sp446.6>
- 1035 Marrett, R., Emerman, S.H., 1992. The relations between faulting and mafic magmatism in
1036 the Altiplano-Puna plateau (central Andes). *Earth and Planetary Science Letters* 112, 53–
1037 59. [https://doi.org/10.1016/0012-821x\(92\)90006-h](https://doi.org/10.1016/0012-821x(92)90006-h)
- 1038 Melnick, D., Echtler, H.P., 2006. Morphotectonic and Geologic Digital Map Compilations
1039 of the South-Central Andes (36°–42°S), in: *The Andes*. Springer Berlin Heidelberg, pp.
1040 565–568. https://doi.org/10.1007/978-3-540-48684-8_30
- 1041 Morabito Garcia, E., & Folguera, A., 2005. El alto de Copahue- Pino Hachado y la fosa de
1042 Loncopué: un comportamiento tectónico episódico, Andes neuquinos (37°- 39°S)
- 1043 Morfulis, M., Báez, W., Retamoso, S., Bardelli, L., Filipovich, R., Sommer, C.A., 2020.
1044 Quantitative spatial distribution analysis of mafic monogenic volcanism in the southern

- 1045 Puna, Argentina: Implications for magma production rates and structural control during its
1046 ascent. *Journal of South American Earth Sciences* 104, 102852.
1047 <https://doi.org/10.1016/j.jsames.2020.102852>
- 1048 Morris, J.D., Leeman, W.P., Tera, F., 1990. The subducted component in island arc lavas:
1049 constraints from Be isotopes and B–Be systematics. *Nature* 344, 31–36.
1050 <https://doi.org/10.1038/344031a0>
- 1051 Mpodosis, C., & Ramos, V. A., 2008. Tectónica jurásica en Argentina y Chile: extensión,
1052 subducción oblicua, rifting, deriva y colisiones. *Revista de la Asociación geológica*
1053 *Argentina*, 63 (4), 481- 497.
- 1054 Munizaga, F., Herve, F., Drake, R., Pankhurst, R.J., Brook, M., Snelling, N., 1988.
1055 Geochronology of the Lake Region of south-central Chile (39°–42°S): Preliminary results.
1056 *Journal of South American Earth Sciences* 1, 309–316. [https://doi.org/10.1016/0895-](https://doi.org/10.1016/0895-9811(88)90009-0)
1057 [9811\(88\)90009-0](https://doi.org/10.1016/0895-9811(88)90009-0)
- 1058 Muñoz, J. & Stern, C., 1985. El complejo volcánico Pino Hachado en el sector nor-
1059 ccidental de la Patagonia (38°- 39°S): volcanismo plio- cuaternario trasarco en
1060 Sudamérica. IV° Congreso Geológico Chileno (Antofagasta), Actas, 3, 381- 412.
- 1061 Muñoz B., J., Stern, C.R., 1988. The quaternary volcanic belt of the southern continental
1062 margin of South America: Transverse structural and petrochemical variations across the
1063 segment between 38°S and 39°S. *Journal of South American Earth Sciences* 1, 147–161.
1064 [https://doi.org/10.1016/0895-9811\(88\)90032-6](https://doi.org/10.1016/0895-9811(88)90032-6)
- 1065 Muñoz, J.B., Stern, C.R., 1989. Alkaline magmatism within the segment 38°-39°S of the
1066 Plio-Quaternary Volcanic Belt of the southern South American Continental Margin. *J.*
1067 *Geophys. Res.* 94, 4545–4560. <https://doi.org/10.1029/jb094ib04p04545>
- 1068 Naipauer, M., Ramos, V.A., 2015. Changes in Source Areas at Neuquén Basin: Mesozoic
1069 Evolution and Tectonic Setting Based on U–Pb Ages on Zircons, in: *Springer Earth*
1070 *System Sciences*. Springer International Publishing, pp. 33–61.
1071 https://doi.org/10.1007/978-3-319-23060-3_3
- 1072 Nakamura, K., 1977. Volcanoes as possible indicators of tectonic stress orientation –
1073 Principle and proposal. *Journal of Volcanology and Geothermal Research*, 2, 1–16.

- 1074 Nelson, E., Forsythe, R., Diemer, J., Allen, M., Urbina, O., 1993. Taitao ophiolite: a ridge
1075 collision ophiolite in the forearc of the southern Chile (46° S). *Revista Geológica de Chile*,
1076 vol. 20. 2, 137-165,
- 1077 Németh, K., Kereszturi, G., 2015. Monogenetic volcanism: personal views and discussion.
1078 *International Journal of Earth Sciences* 104, 2131–2146. [https://doi.org/10.1007/s00531-](https://doi.org/10.1007/s00531-015-1243-6)
1079 015-1243-6
- 1080 Pardo M., Vera E., Monfret T., Yáñez G., Eisenber A., 2006. Sismicidad cortical
1081 superficial bajo Santiago: implicaciones en la tectónica andina y evaluación del pelidro
1082 sísmico, *Actas XI Congreso Geológico Chileno*, vol. 1 pp. 443-446.
- 1083 Pasquare, F.A., Tibaldi, A., 2003. Do transcurrent faults guide volcano growth? The case
1084 of NW Bicol Volcanic Arc, Luzon, Philippines. *Terra Nova*.
1085 <https://doi.org/10.1046/j.1365-3121.2003.00484.x>
- 1086 Paulsen, T.S., Wilson, T.J., 2010. New criteria for systematic mapping and reliability
1087 assessment of monogenetic volcanic vent alignments and elongate volcanic vents for
1088 crustal stress analyses. *Tectonophysics* 482, 16–28.
1089 <https://doi.org/10.1016/j.tecto.2009.08.025>
- 1090 Pérez-López, R., Legrand, D., Garduño-Monroy, V.H., Rodríguez-Pascua, M.A., Giner-
1091 Robles, J.L., 2011. Scaling laws of the size-distribution of monogenetic volcanoes within
1092 the Michoacán-Guanajuato Volcanic Field (Mexico). *Journal of Volcanology and*
1093 *Geothermal Research* 201, 65–72. <http://doi.org/10.1016/j.jvolgeores.2010.09.006ps>
- 1094 Pesce, A., Gimenez, M.E., Gianni, G.M., Folguera, A., Martinez, P., 2019. Magnetic
1095 characterization of a retroarc extensional basin: The Loncopué Trough. *Journal of South*
1096 *American Earth Sciences* 89, 55–62. <https://doi.org/10.1016/j.jsames.2018.11.001>
- 1097 Pesce, A., Gimenez, M. E., Castiglione, B., Gianni, G. M., Folguera, A., 2020. Sección
1098 eléctrica cortical a través de la Fosa de Loncopué. *Revista de La Asociación Geológica*
1099 *Argentina*. 78 (2) 333- 337.
- 1100 Potent S., Reuther C.D., 2001. Neogene Deformationsprozesse im Aktiven magmatischen
1101 Bogen SudCentralChiles zwischen 37° und 39°S. *Mitteilungen aus dem Geologisch-*
1102 *PaleoÉontologischen Institut der UniversitaÉt Hamburg*, 85 pp. 1-2.

- 1103 Rabassa, J., Everson, E., Schlieder, G., Clinch, J. M., Stephens, G. & Zeitler, P., 1987.
1104 Edad Pre- Pleistoceno superior de la glaciación El Cóndor, Valle del Río Malleo, Neuquén.
1105 10° Congreso Geológico Argentino (Tucumán), Actas 4, 217-219.
- 1106 Radic, J. P., Rojass, L., Carpinelli, A., & Zurita, E., 2002. Evolución tectónica de la cuenca
1107 terciaria de Cura- Mallín, región cordillerana chilena argentina (36 30'- 39 00"S). In
1108 Congreso Geológico Argentino 15, 233-241.
- 1109 Ramos, V.A., Folguera, A., 2005. Tectonic evolution of the Andes of Neuquén: constraints
1110 derived from the magmatic arc and foreland deformation. Geological Society, London,
1111 Special Publications 252, 15–35. <https://doi.org/10.1144/gsl.sp.2005.252.01.02>
- 1112 Risse, A., Trumbull, R.B., Coira, B., Kay, S.M., Bogaard, P. van den, 2008. $^{40}\text{Ar}/^{39}\text{Ar}$
1113 geochronology of mafic volcanism in the back-arc region of the southern Puna plateau,
1114 Argentina. Journal of South American Earth Sciences 26, 1–15.
1115 <https://doi.org/10.1016/j.jsames.2008.03.002>
- 1116 Rojas Vera, E.A., Folguera, A., Valcarce, G.Z., Giménez, M., Ruiz, F., Martínez, P.,
1117 Bottesi, G., Ramos, V.A., 2010. Neogene to Quaternary extensional reactivation of a fold
1118 and thrust belt: The Agrio belt in the Southern Central Andes and its relation to the
1119 Loncopué trough (38°–39°S). Tectonophysics 492, 279–294.
1120 <https://doi.org/10.1016/j.tecto.2010.06.019>
- 1121 Rojas Vera, E.A., Sellés, D., Folguera, A., Gimenez, M., Ruíz, F., Orts, D., Zamora
1122 Valcarce, G., Martínez, P., Bechis, F., Ramos, V.A., 2014. The origin of the Loncopué
1123 Trough in the retroarc of the Southern Central Andes from field, geophysical and
1124 geochemical data. Tectonophysics 637, 1–19. <https://doi.org/10.1016/j.tecto.2014.09.012>
- 1125 Rosenau, M.R., 2004. Tectonics of the Southern Andean Intra-arc Zone (38° - 42°S). Freie
1126 Universität Berlin. <https://doi.org/10.17169/REFUBIUM-6146>
- 1127 Ross, P.-S., Delpit, S., Haller, M.J., Németh, K., Corbella, H., 2011. Influence of the
1128 substrate on maar–diatreme volcanoes — An example of a mixed setting from the Pali
1129 Aike volcanic field, Argentina. Journal of Volcanology and Geothermal Research 201,
1130 253–271. <https://doi.org/10.1016/j.jvolgeores.2010.07.018>

- 1131 Schnurr, W.B.W., Risse, A., Trumbull, R.B., Munier, K., n.d. Digital Geological Map of
1132 the Southern and Central Puna Plateau, NW Argentina, in: *The Andes*. Springer Berlin
1133 Heidelberg, pp. 563–564. https://doi.org/10.1007/978-3-540-48684-8_29
- 1134 Schoenbohm, L.M., Carrapa, B., 2015. Miocene–Pliocene shortening, extension, and mafic
1135 magmatism support small-scale lithospheric foundering in the central Andes, NW
1136 Argentina, in: *Geodynamics of a Cordilleran Orogenic System: The Central Andes of*
1137 *Argentina and Northern Chile*. Geological Society of America.
1138 [https://doi.org/10.1130/2015.1212\(09\)](https://doi.org/10.1130/2015.1212(09))
- 1139 Seggiaro, R., Hongn, F., Folguera, A., and Clavero, J., 2006. Hoja Geológica 2769-II, Paso
1140 de San Francisco: Instituto de Geología y Recursos Minerales, Servicio Geológico Minero
1141 Argentino, Boletín 294, 76 p.
- 1142 Sielfeld, G., Cembrano, J., Lara, L., 2017. Transtension driving volcano-edifice anatomy:
1143 Insights from Andean transverse-to-the-orogen tectonic domains. *Quaternary International*
1144 438, 33–49. <https://doi.org/10.1016/j.quaint.2016.01.002>
- 1145 Sigmarsson, O., Condomines, M., Morris, J.D., Harmon, R.S., 1990. Uranium and ^{10}Be
1146 enrichments by fluids in Andean arc magmas. *Nature* 346, 163–165.
1147 <https://doi.org/10.1038/346163a0>
- 1148 Sigmarsson, O., Chmeleff, J., Morris, J., Lopez-Escobar, L., 2002. Origin of ^{226}Ra – ^{230}Th
1149 disequilibria in arc lavas from southern Chile and implications for magma transfer time.
1150 *Earth and Planetary Science Letters* 196, 189–196. [https://doi.org/10.1016/s0012-](https://doi.org/10.1016/s0012-821x(01)00611-2)
1151 [821x\(01\)00611-2](https://doi.org/10.1016/s0012-821x(01)00611-2)
- 1152 Smith, I.E.M., Németh, K., 2017. Source to surface model of monogenetic volcanism: a
1153 critical review. Geological Society, London, Special Publications 446, 1–28.
1154 <https://doi.org/10.1144/sp446.14>
- 1155 Sonder, I., Harp, A.G., Graettinger, A.H., Moitra, P., Valentine, G.A., Büttner, R.,
1156 Zimanowski, B., 2018. Meter-Scale Experiments on Magma-Water Interaction. *J.*
1157 *Geophys. Res. Solid Earth* 123. <https://doi.org/10.1029/2018jb015682>
- 1158 Stern, C.R., 1990. Tephrochronology of southernmost Patagonia. *National Geographic*
1159 *Research*, Vol. 6, p. 110-126.

- 1160 Stern, C.R., 2004. Active Andean volcanism: its geologic and tectonic setting. *Revista*
1161 *geológica Chile* 31. <https://doi.org/10.4067/s0716-02082004000200001>
- 1162 Tadini, A., Bonali, F.L., Corazzato, C., Cortés, J.A., Tibaldi, A., Valentine, G.A., 2014.
1163 Spatial distribution and structural analysis of vents in the Lunar Crater Volcanic Field
1164 (Nevada, USA). *Bull Volcanol.* <https://doi.org/10.1007/s00445-014-0877-8>
- 1165 Tibaldi, A., 1995. Morphology of pyroclastic cones and tectonics. *Journal Geophysical*
1166 *Research* 100, 24521–24535. <https://doi.org/10.1029/95jb02250>
- 1167 Tibaldi, A., Bonali, F.L., Corazzato, C., 2017. Structural control on volcanoes and magma
1168 paths from local- to orogen-scale: The central Andes case. *Tectonophysics.*
1169 <https://doi.org/10.1016/j.tecto.2017.01.005>
- 1170 Tibaldi, A., Bonali, F.L., 2018. Contemporary recent extension and compression in the
1171 central Andes. *Journal of Structural Geology.* <https://doi.org/10.1016/j.jsg.2017.12.004>
- 1172 Trumbull, R.B., Riller, U., Oncken, O., Scheuber, E., Munier, K., Hongn, F., n.d. The
1173 Time-Space Distribution of Cenozoic Volcanism in the South-Central Andes: a New Data
1174 Compilation and Some Tectonic Implications, in: *The Andes*. Springer Berlin Heidelberg,
1175 pp. 29–43. https://doi.org/10.1007/978-3-540-48684-8_2
- 1176 Tunik, M., Folguera, A., Naipauer, M., Pimentel, M., Ramos, V.A., 2010. Early uplift and
1177 orogenic deformation in the Neuquén Basin: Constraints on the Andean uplift from U–Pb
1178 and Hf isotopic data of detrital zircons. *Tectonophysics* 489, 258–273.
1179 <https://doi.org/10.1016/j.tecto.2010.04.017>
- 1180 Turner, J. C., 1973. Descripción de la Hoja 37 ab, Junín de los Andes, provincia del
1181 Neuquén. *Servicio Nacional Minero Geológico, Boletín*, 138, 1-86.
- 1182 Ureta, G., Németh, K., Aguilera, F., Kósik, S., González, R., Menzies, A., González, C.,
1183 James, D., 2021a. Evolution of a magmatic to a phreatomagmatic volcanic system: The
1184 birth of a monogenetic volcanic field, Tilocálar volcanoes, northern Chile. *Journal of*
1185 *Volcanology and Geothermal Research.* <https://doi.org/10.1016/j.jvolgeores.2021.107243>
- 1186 Ureta, G., Németh, K., Aguilera, F., Zimmer, M., Menzies, A., 2021b. A window on
1187 mantle-derived magmas within the Central Andes: eruption style transitions at Cerro Overo

- 1188 maar and La Albóndiga lava dome, northern Chile. *Bull Volcanol.*
1189 <https://doi.org/10.1007/s00445-021-01446-3>
- 1190 Ureta, G, Németh, K, Aguilera, F, Vilches, M, Aguilera, M, Torres, I, Pablo Sepúlveda, J,
1191 Scheinost, A, and González, R, 2021c. An Overview of the Mafic and Felsic Monogenetic
1192 Neogene to Quaternary Volcanism in the Central Andes, Northern Chile (18-28°Lat.S), In:
1193 Németh, K (Ed.) *Updates in Volcanology - Transdisciplinary Nature of Volcano Science*,
1194 IntechOpen, DOI: 10.5772/intechopen.93959. Available from:
1195 <https://www.intechopen.com/chapters/74390>, pp. 249-276
- 1196 Uslular, G., Gençalioglu-Kuşcu, G., Arcasoy, A., 2015. Size-distribution of scoria cones
1197 within the Eğrikuyu Monogenetic Field (Central Anatolia, Turkey). *Journal of*
1198 *Volcanology and Geothermal Research* 301, 56–65.
1199 <https://doi.org/10.1016/j.jvolgeores.2015.05.006>
- 1200 Uslular, G., Le Corvec, N., Mazzarini, F., Legrand, D., Gençalioglu-Kuşcu, G., 2021.
1201 Morphological and multivariate statistical analysis of quaternary monogenetic vents in the
1202 Central Anatolian Volcanic Province (Turkey): Implications for the volcano-tectonic
1203 evolution. *Journal of Volcanology and Geothermal Research* 416, 107280.
1204 <https://doi.org/10.1016/j.jvolgeores.2021.107280>
- 1205 Varekamp, J.C., Hesse, A., Mandeville, C.W., 2010. Back-arc basalts from the Loncopue
1206 graben (Province of Neuquen, Argentina). *Journal of Volcanology and Geothermal*
1207 *Research* 197, 313–328. <https://doi.org/10.1016/j.jvolgeores.2010.04.003>
- 1208 Vergani, G. D., Tankard, A. J., Belotti, H. J., & Welsink, H. J., 1995. Tectonic evolution
1209 and paleogeography of the Neuquén Basin, Argentina. *American Association of Petroleum*
1210 *Geologists, Memoir* 62, 383-402.
- 1211 Vergara, M., & Muñoz, J., 1982. La Formación Cola de Zorro en la alta cordillera Andina
1212 Chilena (36-39 Lat. S), sus características petrográficas y petrológicas: Una revisión.
1213 *Revista Geológica de Chile*, 17 (1), 31-46.
- 1214 Wood, C.A., 1979. Monogenetic volcanoes of the terrestrial planets. *Proceedings of the*
1215 *10th Lunar and Planetary Science Conference*, Houston, Texas, March 19–23. vol. 1979.
1216 Pergamon Press, Inc., New York, pp. 2815–2840.

- 1217 Zhao, Y.-W., Fan, Q.-C., Zou, H.-B., Li, N., 2019. Tectonic controls of Late Cenozoic
1218 monogenetic intraplate volcanism at the Wulanhada volcanic field, Northern China.
1219 *Journal of Volcanology and Geothermal Research* 383, 16–27.
1220 <https://doi.org/10.1016/j.jvolgeores.2018.01.022>
- 1221 Zannettini, J. C. M., Leanza, H. A., Giusiano, A., Santamaría, G. R., & Franchi, M., 2010.
1222 Hoja Geológica 3972- II Loncopué. Servicio Geológico Minero Argentino (SEGEMAR)
1223 Boletín N° 381, 93.
- 1224 Zarazúa-Carbajal, M.C., De la Cruz-Reyna, S., 2020. Morpho-chronology of monogenetic
1225 scoria cones from their level contour curves. Applications to the Chichinautzin
1226 monogenetic field, Central Mexico. *Journal of Volcanology and Geothermal Research* 407,
1227 107093. <https://doi.org/10.1016/j.jvolgeores.2020.107093>